Dynamical and Structural Properties of Hydrophobically Modified Pluronic PCL-F127-PCL

Natalie Solfrid Gjerde

Master thesis in Chemistry
60 credits

Department of Chemistry
Faculty of Mathematics and Natural Sciences
UNIVERSITY OF OSLO

June 2017

Dynamical and Structural Properties of Hydrophobically Modified Pluronic PCL-F127-PCL

By

Natalie Solfrid Gjerde

Supervisor:

Bo Nyström

Co-supervisor:

Sandra Medel

Department of Chemistry

Faculty of Mathematics and Natural Sciences

UNIVERSITY OF OSLO

June 2017

2017

Dynamical and Structural Properties of Hydrophobically Modified Pluronic PCL-F127-PCL

Natalie Solfrid Gjerde

http://www.duo.uio.no/

Printed at Reprosentralen, Universitetet i Oslo

Abstract

In this thesis, structural and dynamic features of thermoresponsive amphiphilic pentablock copolymers have been studied for their potential use for drug delivery application. The copolymers are amphiphilic poly(ethylene oxide)-poly(propylene oxide)-poly(ethylene oxide) (PEO-PPO-PEO), also known as Pluronic, modified with hydrophobic poly(caprolactone) (PCL) to give the pentablock terpolymer PCL-PEO-PPO-PEO-PCL (PCL_n-Pluronic-PCL_n). The effects of the PCL length (n = 5 and 11) on the self-assembly properties of PCL-Pluronic-PCL in aqueous solutions have been investigated at various temperatures and both in the dilute and the semidilute concentration regimes.

Turbidity measurements revealed a lower critical solution temperature, where the cloud point decreased with PCL length. Through dynamic light scattering (DLS) measurements, the polymers were found to form a mixture of micelles and intermicellar aggregates. A longer PCL length resulted in larger intermicellar aggregates. Small angle neutron scattering (SANS) measurements revealed that the polymers with a short PCL length formed spherical flower-like micelles, whereas the polymers with a long PCL length formed elongated cylindrical micelles.

In the semidilute concentration region, the polymers form thermoreversible hydrogels at elevated temperatures. The gel window in the phase diagrams for these polymers greatly depends on the PCL length, where a longer PCL length decreases the concentration and temperature needed for gelation. The dynamic properties of the gels were characterized by rheology. SANS measurements revealed a tight ordering of the micelles in these systems, and demonstrated interesting conformational differences between the systems.

Acknowledgement

First of all, I would like to thank my supervisor Bo Nyström for your continuous support and encouragement. Your incredible knowledge has been invaluable for this study, and I cannot thank you enough for always having your door open for inspiring discussions. I have learned so much through your guidance.

I would also like to give a big thank you to my co-supervisor Dr. Sandra Medel. Not only have you taught me so much, but your continuous support and help during my stressful times has meant a lot to me.

I would like to give a big thank you to Kenneth D. Knudsen for working with my polymers and helping me understand how they work. I would also like to thank Dr. Kaizheng Zhu for synthesizing the polymers studied in this thesis. Thank you to Dr. Thomas Zinn for showing me how to use the rheometer. I would also like to thank Dr. Sara Bekhradnia for showing me how to analyze the DLS results.

I would like to give a big thank you to Barbara Claro for teaching me so many things during your short stay. Not only are you a great teacher, but also a great friend.

A big thank you goes to the polymer group for always motivating me and giving me great advices.

For my incredible friends, I am forever grateful for having you around. Your jokes and cheering never fail to brighten my mood. Life would not be the same without you.

To Wei Fang, thank you for always being by my side. I love you.

Last but not least, I would like to thank my incredible parents. No words can describe how grateful I am for your endless amount of love and support. You are my inspiration.

Abbreviations

ºC	degree Celsius
A_0	area of the hydrophilic block on the interface
A_f	amplitude of the fast mode
A_s	amplitude of the slow mode
B	instrumental factor
c	polymer concentration
CGC	critical gelation concentration
CGT	critical gelation temperature
CMC	critical micelle concentration
CMT	critical micelle temperature
CP	cloud point
d	characteristic distance
d_f	fractal dimension
D	diffusion coefficient
DLS	dynamic light scattering
FDA	U.S. Food and Drug Administration
F127	Pluronic where PEO constitutes 70% of the block copolymer
G*	complex modulus
G'	storage modulus
G"	Loss modulus
$g^1(t)$	first order electric field autocorrelation
$g^2(t)$	second order intensity autocorrelation
I(q)	scattering intensity

k_B	Boltzmann constant
k_i	incident wave vector
k_s	scattered wave vector
LCST	lower critical solution temperature
LVE range	linear viscoelastic range
n	refractive index
n	the relaxation exponent
n	number of repeating monomer units
N	aggregation number
l_c	hydrophobic tail length
L	characteristic length of polymer system
LVE	linear viscoelastic range
Mn	number average molecular weight
Mw	weight average molecular weight
p	packing parameter
P(q)	form factor
PBO	poly(oxybutylene)
PCL	poly(caprolactone)
PCS	photon correlation spectroscopy
PDI	polydispersity index
PEO	poly(ethylene oxide)
PPO	poly(propylene oxide)
QUELS	quasi elastic light scattering
q	scattering vector
R_c	radius of the core
X	

R_g	radius of gyration
R_h	hydrodynamic radius
ROP	ring opening polymerization
S(q)	structure factor
SANS	small angle neutron scattering
SAS	small angle scattering
SAOS	small amplitude oscillatory shear
SLS	static light scattering
t	time
T	temperature in Kelvin
tan δ	damping tangent
UCST	upper critical solution temperature
v	hydrophobic tail volume
V	scattering volume
wt%	weight percent
β_f	the width of relaxation times, fast mode
β_s	the width of relaxation times, slow mode
Γ	gamma function
γ	strain amplitude
δ	phase lag
η	viscosity
η*	complex viscosity
θ	scattering angle
λ	wave length
ρ_1, ρ_2	scattering length densities

σ	shear stress
τ	turbidity
τ_f	fast relaxation time
τ_s	slow relaxation time
τ_{se}	single exponent relaxation time
ω	angular frequency

Table of Contents

1 Introduction

During the past few decades, amphiphilic block copolymers with the ability to self-assemble into nanostructured species like micelles or vesicles in aqueous media, have received a great amount of interest in the field of controlled drug delivery [1-3]. By forming micelles that have a hydrophobic core and a hydrophilic shell, hydrophobic drugs that are otherwise poorly soluble in the body's physiological conditions can be stored within the micelles. The hydrophilic shell of the micelles then enhances the solubility of the hydrophobic drugs [4]. Furthermore, it has been found that particles of less than 200 nm in size are able to avoid protein opsonization due to their high curvature [5]. Thus, problems such as protein adsorption and subsequent macrophage uptake can be circumvented, allowing prolonged circulation time and more effective treatment [6]. The advantages of using polymers as drug carriers are hence evident.

For sustained release drug delivery, hydrogels that act as drug deposits are of great interest [7, 8]. By introducing a gel network made of drug containing micelles under the patient's skin, drugs can slowly be released into the bloodstream as the gel decomposes. These micelles can then travel through the bloodstream and bring the drugs to the diseased tissue[9]. Drug deposits would relieve the patient of the inconvenience and distress of having to regularly visit the doctor's office for a new drug dose.

Hydrogels that possess thermoreversible gelation are of special interest in the field of sustained drug release [10, 11]. With the feature of being a low viscosity liquid at low temperatures and a semi-solid gel at temperatures close to the body's temperature, these systems can easily be injected into the patient through a syringe, making the process of drug deposit introduction much easier.

Poly(ethylene oxide)-*b*-poly(propylene oxide)-*b*-poly(ethylene oxide) (PEO-PPO-PEO) triblock copolymers, also known as Pluronic or Poloxamer, are amphiphilic triblock copolymers that have received much interest in the biomedical field [12-14]. Due to the dehydration of PPO at elevated temperatures, these polymers display thermoreversible self-assembly into micelles [15, 16]. Furthermore, at high enough concentrations (typically $c > 15$ wt%) Pluronic micelles arrange themselves into ordered structures, e.g., cubic lattices [17-20],

which results in the formation of thermoreversible hydrogels. Pluronics are cheap to produce, easy to modify, and already approved by the Food and Drug Administration (FDA) for pharmaceutical and biomedical applications. Thus, Pluronic gels are interesting candidates for sustained-release drug delivery.

The main drawback with Pluronic gels is their rapid dissolution rate in aqueous media. Usually, they dissolve within a couple of days after injection [21-23]. For the purpose of sustained release, where the ideal dissolution rate would be at least a couple of months, Pluronic gels are therefore not adequate. Several methods to stabilize the gels have been studied, e.g., covalently or physically cross-linking the gel network [24, 25], mixing with other polymers [22], or chemically modifying the polymer [26]. However, another strategy could potentially be the answer. The rapid dissolution rate of Pluronic gels is owed to their low mechanical strength. The main mechanism behind their gelation is through hydrophobic associations. However, PPO's hydrophobicity is quite low. A strategy of attaching hydrophobic blocks at each end of Pluronic could potentially enhance the hydrophobic associations in the gel network and make it stronger and less easy to dissolve in aqueous media.

A good candidate for hydrophobically modifying Pluronic is poly(caprolactone) (PCL). PCL has already found extensive use in the biomedical field due to its excellent biocompatibility and biodegradable nature [27, 28]. Furthermore, Pluronic/PCL block copolymers have been found to have low cytotoxicity [29, 30]. Several studies for biomedical applications have been done on various Pluronic/PCL systems, e.g., as porous membranes for enhanced guided bone regeneration [31], for treatment of glottal insufficiency [32], or as nanocarriers for antioxidants and proteins [33, 34]. However, there is a lack of studies on the self-assembly behavior and hydrogels formed by Pluronic/PCL pentablock copolymers. It is therefore interesting to investigate the properties and potential of Pluronic/PCL systems.

1.1 Aim of Project

For this project, pentablock copolymers composed of Pluronic F127 and PCL (PCL-F127-PCL) have been studied. To check the ideal length of PCL, two different F127/PCL samples, one with 5 repeating units of PCL and the other with 11 repeating units, were measured and compared against each other. In addition, as a reference, experiments were also performed on the original F127 copolymer.

To properly understand the behavior of PCL modified F127, the study was divided into two parts. The first part focuses on the self-assembly of the polymers. Properties such as thermodynamics, aggregation sizes, the width of size distribution, and micellar structures were probed by conducting turbidity, dynamic light scattering (DLS), and small angle neutron scattering (SANS) experiments on dilute solutions. The second part of the study focuses on the gelation properties of the polymers in the semidilute concentration regime. To get an overview of the macroscopic behavior of the polymer solutions, a phase diagram was constructed. The viscoelastic properties of semidilute solutions were measured by rheology, while the morphological features of these samples were probed by SANS experiments.

2 Theory and Background

2.1 Block Copolymers

Block copolymers are composed of at least two or more blocks of chemically different monomers. These blocks can be connected together in a linear and/or radial arrangement, giving rise to different block copolymer architectures [35], as illustrated in Figure 1. The simplest block copolymers are composed of only two different homopolymers and form linear AB diblock copolymers, where A and B represent the respective monomers forming the block copolymer. By attaching another block of monomer, a triblock copolymer is formed etc. This could either be an ABA triblock copolymer, or BAB or even ABC [36-38]. The interesting self-assembly properties of triblock copolymers will be explored later in the chapter.

2.1.1 Amphiphilic Block Copolymers

Amphiphilic block copolymers are copolymers composed of at least one hydrophilic block and one hydrophobic block. Due to the different solubility of these blocks in selective solvents, e.g. aqueous solutions, amphiphilic block copolymers can self-assemble into several interesting nanostructures, depending on the nature and composition of the individual blocks composing the copolymer [17, 39]. In this study, focus will be on the properties and self-assembly behavior of linear amphiphilic block copolymers.

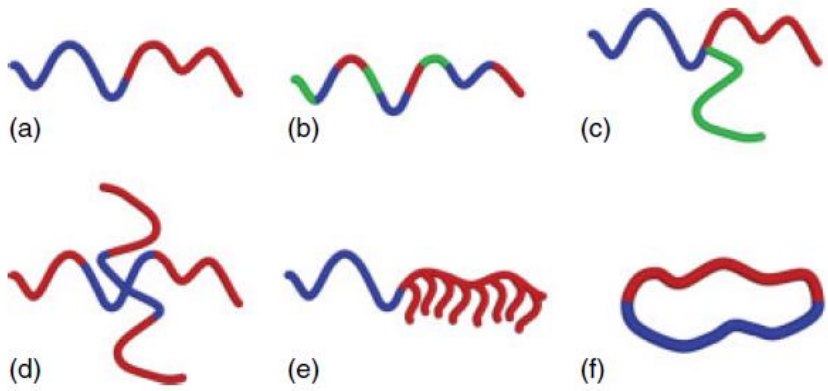

Figure 1. Illustration of the different architectures of block copolymers borrowed from Adams et al [40]. a) Linear diblock copolymer, b) linear multiblock copolymer, c) miktoarm copolymer, d) star copolymer, e) linear-graft copolymer, and f) cyclic diblock copolymer. The different colors represent different monomer blocks.

2.1.2 Temperature Responsive Block Copolymers

Some polymers possess a temperature sensitive characteristic [41]. These polymers are soluble in a certain temperature range, whereas at other temperatures they are insoluble. This is a very interesting property for drug delivery purposes, as the incorporation of these kinds of polymers into drug delivery systems gives rise to self-assembly properties that can be controlled by external temperature [42].

Mainly, there are two types of thermoresponsive polymers [43]. The first type are polymers that possess a phase diagram with a lower critical solution temperature (LCST) behavior. These polymers are miscible in the solvent *below* the LCST, while immiscible above it, e.g., PPO in Pluronic [15]. Their immiscibility can be observed by a cloudy solution, due to a macroscopic phase separation of the polymers. The temperature where the macroscopic phase separation occurs (for a specific polymer concentration) is therefore often referred to as the cloud point (CP). The second type are polymers that have an upper critical solution temperature (UCST). In contrast to the first type, these polymers are miscible *above* the UCST, while immiscible below it. Figure 2 illustrates the typical phase diagrams of polymers with a LCST feature and polymers with an UCST.

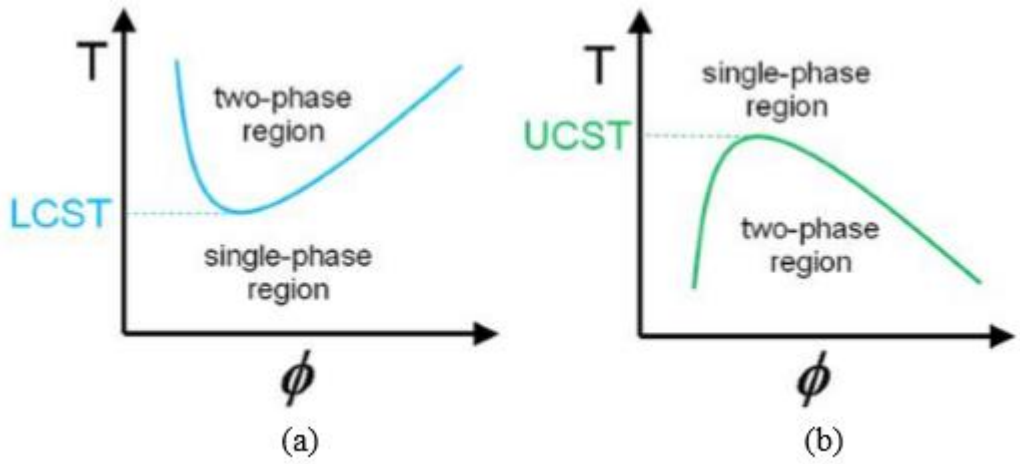

Figure 2. Temperature vs. polymer volume fraction, Φ. A schematic illustration of the phase diagrams of polymer solutions with a) LCST behavior and b) UCST behavior. Illustration borrowed from Ward et al [44].

Both thermoresponsive characteristics are driven by thermodynamic forces. In the case of polymers with a LCST, the phase separation is an entropically driven process. More specifically, it is driven by the entropy of water [45]. Below the LCST, the polymer chains are solved in the aqueous solution by forming hydrogen bonds with the surrounding water molecules. However, as the solution is heated, it becomes energetically unfavorable for the water molecules to remain ordered with the polymer chains. The hydrogen bonds consequently break and the polymers dehydrate, becoming hydrophobic and phase separating out of the solvent due to the hydrophobic effect [46]. The UCST, on the other hand, is an enthalpically driven process [47].

In addition of having a critical micelle concentration criterion, CMC, amphiphilic block copolymers with thermoresponsive polymers in their composition, usually have a critical micelle temperature (CMT) self-assembly criterion [48]. For drug delivery purposes, polymers with LCST properties are of most interest.

2.1.3 Pluronic - F127

Pluronic is the trademark name of triblock ABA block copolymers composed of poly(ethylene oxide)$_a$–poly(propylene oxide)$_b$–poly(ethylene oxide)$_a$ (PEO_a-PPO_b-PEO_a). These also go under the name Poloxamer. Due to the hydrophilic nature of PEO and the dehydration of PPO at elevated temperatures, these block copolymers display interesting thermoresponsive self-assembly properties [16, 49]. With the ease of tuning the self-assembling properties by varying the composition of the copolymer, i.e., molecular weight and relative block length [14, 50], Pluronics have found a wide variety of applications in the industrial field. With PEO's highly hydrophilic nature and its well-known good blood compatibility [51, 52], Pluronics have also garnered much interest in the biomedical field, for applications such as tissue scaffolds and drug delivery [14, 53].

F127 is a Pluronic sample where PEO constitutes 70% of the block copolymer (see Figure 3). With this high content of PEO, F127 possesses good biocompatibility and advantages such as avoiding protein adsorption and subsequent macrophage uptake [51]. This, in combination with F127's temperature sensitive self-assembly and gelation properties, have made F127 an excellent candidate for biomedical applications.

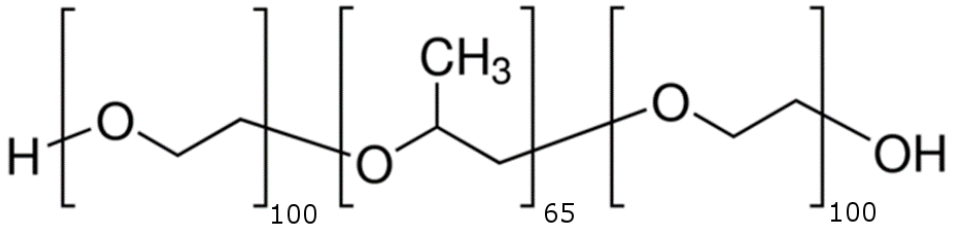

Figure 3. Molecular composition of Pluronic F127 as given by the manufacturer.

2.1.4 Poly(caprolactone)

Poly(caprolactone) (PCL) is an aliphatic polyester, which is hydrophobic and semi-crystalline. PCL has an excellent biocompatible and biodegradable nature [27, 54], and is found to have a good blend-compatibility with a wide range of polymers and drugs [55]. With this good blend-compatibility, PCL can act as drug carriers making them especially interesting for drug delivery purposes. PCL has found extensive applications in the biomedical field, especially for tissue engineering [56].

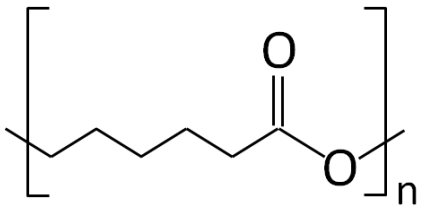

Figure 4. Molecular structure of PCL, where n represents the number of repeating monomer units.

2.1.5 Self-Assembly of Amphiphilic Block Copolymers in Aqueous Solutions

Self-assembly of amphiphilic block copolymers is a thermodynamically driven process, arising from one of the blocks in the copolymer being poorly solved by the solvent [39]. In aqueous solutions, the hydrophobic parts of the copolymers are negative to water and consequently want as little contact with it as possible. In order to minimize the free energy of the system arising from this unfavorable interaction, the block copolymers orientate

themselves to remove the hydrophobic parts from the aqueous solution. If the concentration of polymers is high enough, above CMC, the block copolymers self-assemble into micelles. These micelles usually have a diameter from 10 nm to 100 nm, and are characterized by a core-shell architecture, where the core is composed of the hydrophobic blocks, while the shell is composed of the hydrophilic blocks [49, 57, 58]. Figure 5 illustrates the self-assembly of amphiphilic diblock copolymers into micelles, and their ability to carry hydrophobic drugs in their core. Below the CMC, the copolymers exist as individual polymer chains (unimers). The formation of micelles is a reversible process, where an equilibrium of unimers entering and exiting the micelles is maintained [39].

Typically, polymeric micelles have a CMC in the order of 10^{-6}-10^{-7} M [59]. Surfactants, which also self-assemble into micelles due to their similar amphiphilic nature, usually have CMC around 10^{-3}-10^{-4} M [60]. Polymeric micelles are thus more resistant to dilution than surfactant micelles, which is an important feature for drug delivery, as the micelles will experience extreme dilution when introduced into the bloodstream. It is crucial that the micelles don't disintegrate and release the drugs before they reach their targeted tissue.

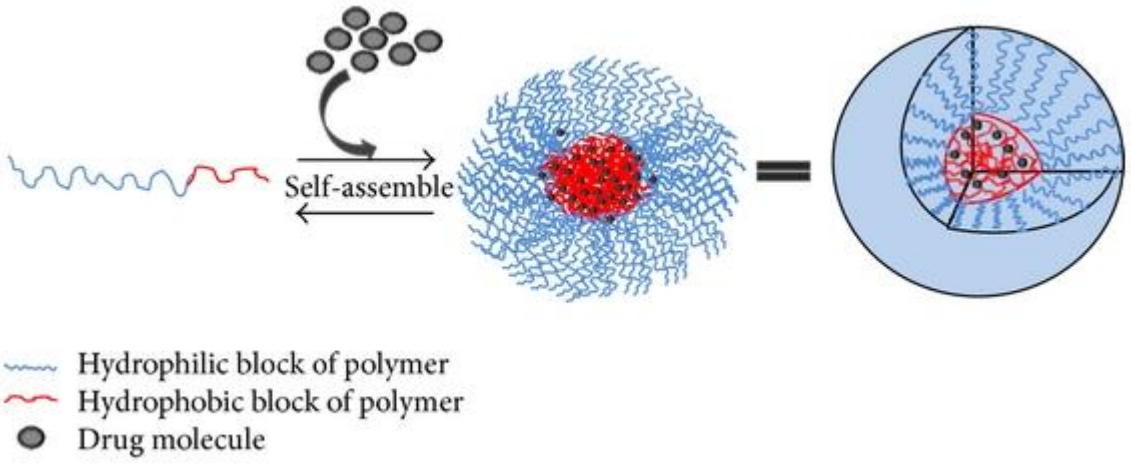

Figure 5. A schematic illustration of the self-assembly of amphiphilic diblock copolymers into micelles, and their ability to carry hydrophobic drug molecules in the hydrophobic core. Image borrowed from Xu et al [61].

2.1.6 Micellar Morphology

As already mentioned, amphiphilic block copolymers can form micelles with a wide variety of morphologies. There are several factors affecting the morphology of the micelles, e.g., the composition of the copolymer, the lengths and properties of each respective block, or even external conditions such as concentration, temperature, or the addition of salts [50, 62-64].

In 1976, J. Israelachvili et al. developed a simple geometric approach to predict the micellar morphology formed by surfactants [65]. Primarily, two opposite forces control the micelle formation: the attractive forces between the hydrophobic tails, which lead to aggregation, and the repulsive forces between the polar heads, which prevent unlimited growth of the micelles. How strong the hydrophobic attraction is, will depend on the length (l_c) and volume (v) of the hydrophobic tail, while the strength of the repulsive forces between the polar heads, will depend on the interfacial area of the molecule (a_o). From this, J. Israelachvili defined a non-dimensional packing parameter:

$$p = \frac{v}{a_0 l_c} \qquad (1)$$

Although the packing parameter was originally derived for surfactants, it is often used to generally explain the morphology of polymeric micelles. Figure 6 illustrates the different morphologies predicted by p. When $p < 1/3$, the volume of the hydrophobic block is small relative to the hydrophilic block, and the individual molecules have a cone shape. This results in the formation of spherical micelles. As the hydrophobic block becomes bigger and occupies a larger volume, p accordingly increases. For $1/3 < p < 1/2$, cylindrical micelles are formed. For even higher p, bilayered structures are formed.

The packing parameter thus gives a general idea of how changing the length of the hydrophobic or hydrophilic blocks affects the resulting micellar morphologies.

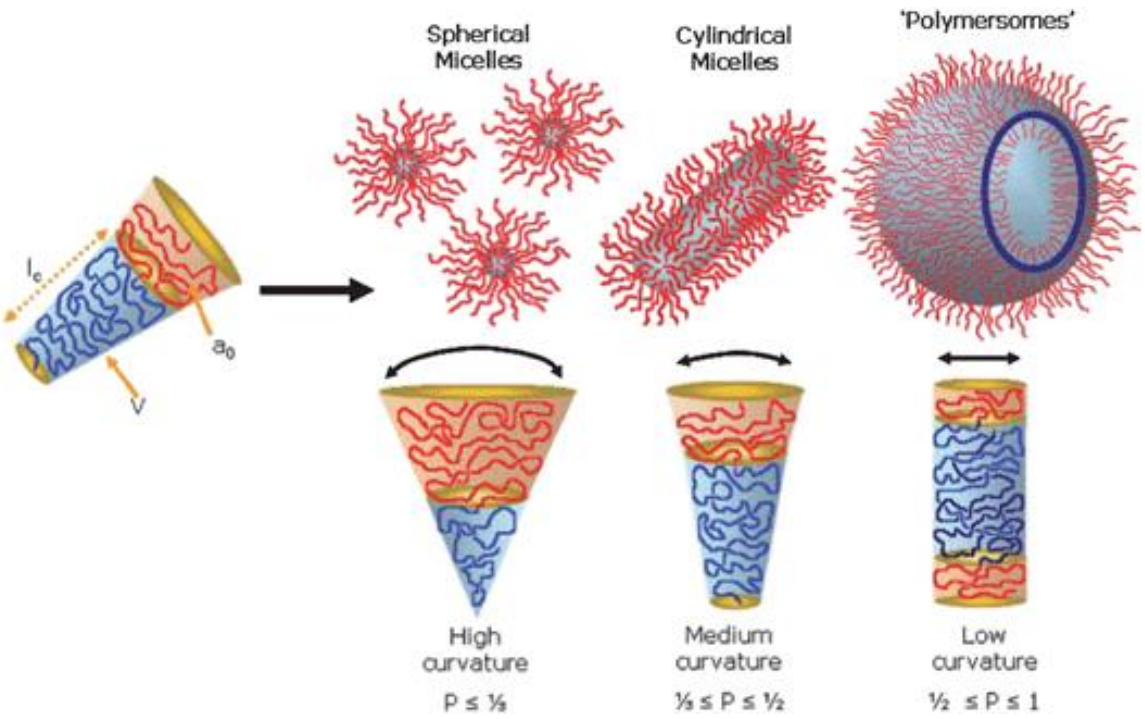

Figure 6. Illustration of how the packing parameter, *p*, predicts the micellar morphology. The picture is borrowed from Adams et al [40].

2.1.7 Self-Assembly of A-B-A vs. B-A-B Triblock Copolymers

In chapter 2.1.5, it was explained how amphiphilic block copolymers self-assemble in selective solvents. The self-assembly of an amphiphilic diblock copolymer was used as an example. However, adding another block to the block copolymer can result in very different self-assembly properties. A great example of this are amphiphilic triblock copolymers. These display very different self-assembly properties depending on their block composition [66]. Take for example ABA triblock copolymers, where A is a hydrophilic block and B hydrophobic. When these are dissolved in water, the B blocks arrange themselves into micellar cores, while the A blocks remain in contact with the solvent and form the micellar corona. Due to the highly hydrophilic corona, these micelles are repulsed by each other and tend to behave as individual micelles. However, if the blocks are rearranged into BAB triblock copolymers, a very different behavior appears. When these polymers are dissolved in water, the B blocks still want to migrate into the micellar cores. However, for them to be able to both hide in the core, the middle A block needs to be bent into a loop structure. This leads to the formation of flower-like micelles (see Figure 7a). An important factor for the formation of flower-like micelles is the flexibility of the middle A block. If the A block is sufficiently

long and flexible, both B blocks can be hidden in the micelle core. In this case, the micelles act as individual micelles similar to those formed by ABA triblock and diblock copolymers. However, if the A block is not able to form a loop, a B block can end up dangling outside in the solvent (Figure 7b). Micelles with exposed dangling B blocks can experience attractive forces between the dangling hydrophobic blocks. Furthermore, if the A block is long enough, the dangling B blocks can migrate into other micelle cores leading to the formation of branched structures (Figure 7c). Connectivity between micelles leads to very different behavior between ABA and BAB triblock copolymers systems.

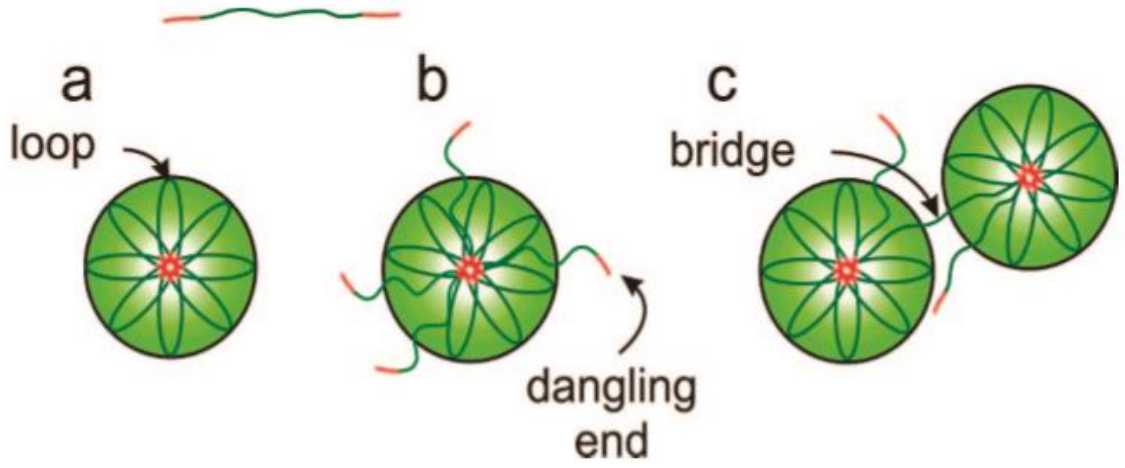

Figure 7. Most probable types of organization of ABA triblock copolymers in B-selective solvents. Picture borrowed from Giacomelli et al [66].

2.2 Polymeric Hydrogels

Hydrogels are hydrophilic three-dimensional polymer networks that can absorb up to thousands of times their dry weight in water [7, 67]. Hydrogels can be made from synthetic or natural polymers, or even a combination of the two. Due to their high water content and their physiochemical similarity to the native extracellular matrix, hydrogels are generally considered to be highly biocompatible [68]. This has given them several applications in the biomedical field [69-71]. Specifically, hydrogels are very interesting for drug delivery purposes due to their highly porous structure. Within these pores drugs can be stored and

hydrogels can then act as drug depots. By slowly eluting out of the gel matrix, a high local concentration of drugs can be maintained in the surrounding tissues over an extended period of time, making hydrogels candidates for sustained drug delivery [23, 72].

Hydrogels are mainly divided into two categories, either physical or chemical gels. *Physical* gels, also called reversible gels, are formed through intermolecular associations, by weak secondary forces such as ionic, H-bonding or hydrophobic forces [73, 74]. These interactions are often reversible and can be disrupted or induced by changes in the physical conditions such as temperature, pH or application of stress. Physical gels can thus be stimuli-responsive. *Chemical* gels, also called permanent gels, are hydrogels with covalently crosslinked networks [75]. Due to the strong forces connecting the network, these gels are chemically stable and non-reversible, making them much stronger than physical gels.

2.2.1 Thermoresponsive Hydrogels

Thermoresponsive hydrogels are physical gels that display an interesting temperature induced sol-gel transition. During a sol-gel transition, a polymer solution goes from being a low viscous solution at low temperatures to a semi-solid gel at elevated temperatures. This feature is very interesting for drug delivery purposes, as this enables the introduction of a drug depot through a simple, non-invasive injection with a syringe.

Thermoresponsive hydrogels are usually composed of block copolymers with at least one block possessing a LCST behavior [76, 77]. These polymer solutions are low viscosity liquids below the LCST due to the hydrophilic nature of the copolymer. However, as the solution is heated, the copolymer dehydrates and becomes hydrophobic. The main driving force behind the gelation of thermoresponsive hydrogels is hydrophobic associations. In these gel networks, a delicate balance between swelling hydrophilic blocks and aggregating hydrophobic blocks is achieved [78]. Figure 8 illustrates the gelation mechanism by hydrophobic interactions.

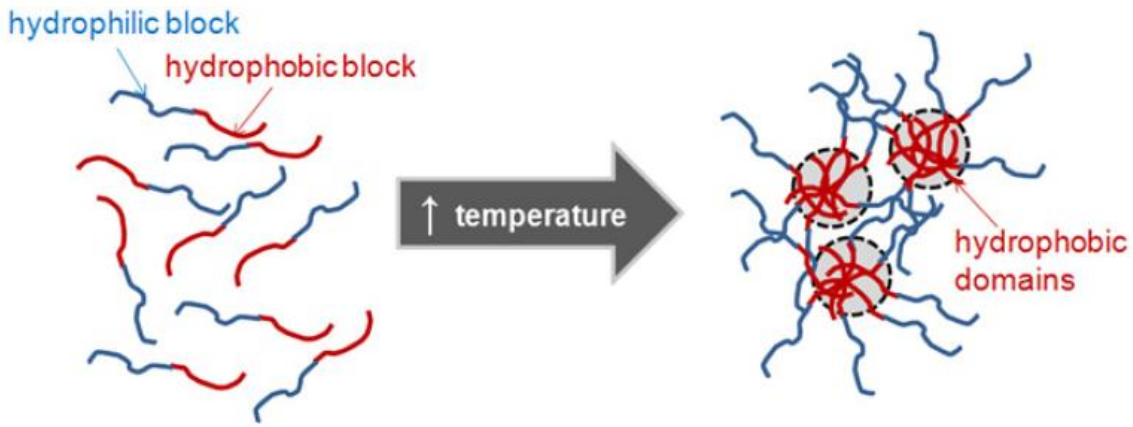

Figure 8. Illustration of physical gelation driven by hydrophobic associations. Borrowed from Hoare et al [67].

For thermoresponsive hydrogels, there are two critical criteria describing the gelation. The first criterion is that the concentration of polymers needs to be high enough to create a network expanding throughout the whole solution. This is called the critical gelation concentration (CGC). The second criterion is that the temperature needs to be high enough to form the gels. This is called the critical gelation temperature (CGT). These two properties can be tuned by changing the molecular composition[79], or by adding salts or additives to the polymer solutions [80, 81].

2.2.2 Gelation of F127

The polymer studied in this project, Pluronic F127, is a perfect example of a thermoresponsive hydrogel forming polymer. The gelation of these systems has been studied in great detail by several methods [49, 82, 83]. K Mortensen, who was written several articles on Pluronics, has studied the gel formation through SANS and cryo-TEM experiments, and explained it by a cubic close packing of spherical micelles at elevated temperatures [18]. Like other thermoresponsive hydrogels, the CGC and CGT of F127 depend on physical conditions such as concentration, pH, or addition of salts or additives [62, 81].

2.3 Characterization Methods

In this section, the basic theory behind the instruments used is explained.

2.3.1 Turbidimetry

In section 2.1.2, the phase separation curve of polymers with an LCST was discussed. It was said that at a specific concentration, the temperature at which the polymer phase separates is defined as the cloud point (CP). This is one of the most important parameters for application of thermoresponsive polymers. Thus, methods to determine it are necessary.

Turbidimetry is an extensively used method to determine a polymer's CP. The basic principle of the turbidimetry instrument used in this study is to detect light scattered by phase separated polymers. A schematic illustration of the instrument setup is shown in Figure 9. The polymer solution is placed on a mirror. A light beam is then focused on it. As the solution is heated, an optical detector, positioned 180° above it, continuously detects any scattered light. When the polymers are hydrophilic and solved in the solution, the light simply passes through the solution and reflects from the mirror. However, as the polymers phase separate at elevated temperatures, the light beam collides with them and becomes scattered. The scattered light then hits the detector, causing an abrupt increase in the measured scattered intensity.

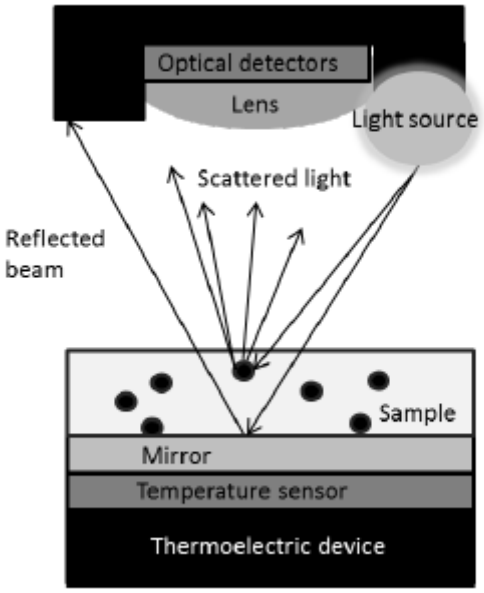

Figure 9. Schematic illustration of a cloud point analyzer.

The scattered intensity signal can be related to the turbidity curve by the empirical equation [84]:

$$\tau = 9.0 \cdot 10^{-9} S^{3.751} \quad (2)$$

where τ is the turbidity and S is the signal. The CP is then defined as the temperature at which the turbidity curve rises from the baseline.

2.3.2 Scattering Techniques

Scattering techniques are powerful tools in the characterization of molecular structures in colloidal systems [85, 86]. Quantitative information such as size, shape and structure of e.g. individual polymer coils, micelles, or even larger particles can be obtained. These techniques are based on the interaction of particles in solution with incident radiation (e.g., light, X-ray or neutrons). Which scattering source that best probes the colloidal system is determined by the size and scattering properties of the particles. In general, light sources are usually used to probe larger particles (20 nm – 2.5 μm), while X-rays or neutrons are useful to probe smaller particles (1 Å – 50 nm).

Common for scattering methods is that the length scale that they probe is determined by the wave vector, $\vec{q}$ (see Figure 10). $\vec{q}$ is related to the scattering angle via:

$$\vec{q} = \overrightarrow{k_s} - \overrightarrow{k_i} \quad (3)$$

where $\overrightarrow{k_i}$ is the initial wave vector and $\overrightarrow{k_s}$ is the scattered neutron wave vector [87]. For completely elastic scattering, its magnitude can be expressed as:

$$q = \frac{4\pi \mathrm{n}}{\lambda} \sin\left(\frac{\theta}{2}\right) \quad (4)$$

where n is the refractive index of the solvent, λ is the wavelength of the incident light, and θ is the scattering angle. Thus, by varying either λ or θ, different length scales can be probed.

For small angle scattering (SAS) techniques, the scattering angle is usually set to 2θ and n = 1 [87]. In these cases, the distance probed is directly proportional to q by:

$$d = \frac{2\pi}{q} \quad (5)$$

where d is the distance probed.

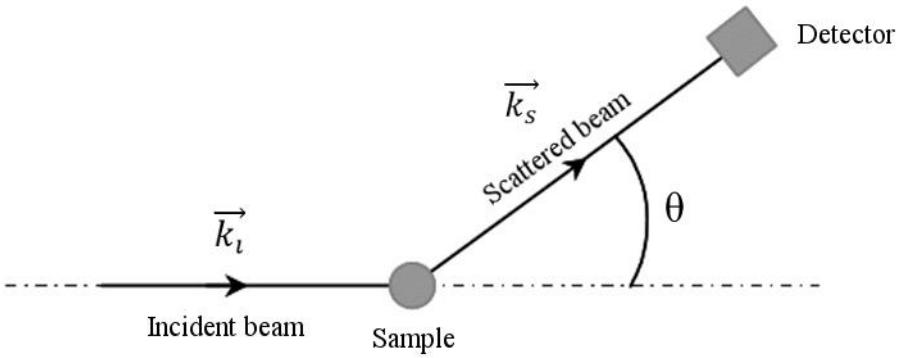

Figure 10. Schematic instrumental setup of scattering techniques.

For polymer systems, it is useful to know whether it is the global structure of the system that is seen, e.g., the shape of the polymers in solution, or if it is the local structure of the system which is probed. The dimension probed is related to the quantity qL, where L is the characteristic length of the polymer system. For dilute systems L is defined as R_g (radius of gyration) or R_h (hydrodynamic radius), while in semidilute systems it is the mesh size, ξ. When $qL < 1$ the global dimension is probed, while for $qL > 1$ the local structure is probed [88].

2.3.3 Dynamic Light Scattering

Dynamic light scattering (DLS), also known as Quasi-Elastic Light Scattering (QELS) or Photon Correlation Spectroscopy (PCS), is a light scattering technique that characterizes the size and the width of the size distribution of particles in solution [86]. The q-range probed is between 0.0005 to 0.005 $Å^{-1}$, corresponding to a length scale of 20 to 200 nm. However, an approximate range from 2 nm to 2 nm can be probed, making DLS good for studying particles on a mesoscopic scale.

Sizes are determined with DLS through the assumption that particles display Brownian motion in solution (due to constant collisions with adjacent solvent molecules). By monitoring how fast the particles move in and out of the illuminated area, DLS can indirectly measure their diffusion coefficient, D. Assuming that the particles are spherical, the hydrodynamic radius, R_h, can then be determined through the Stokes-Einstein equation [89]:

$$D = \frac{kT}{6\pi\eta R_h} \quad (6)$$

where k is the Boltzmann constant, T is the sample temperature, and η is the solvent's viscosity.

In detail, DLS quantitatively analyzes the motion of the particles by monitoring the fluctuating scattered intensity, arising from the particles moving in and out of the scattering volume. The scattered intensity fluctuations are then expressed in terms of time-intensity-autocorrelation functions, $g^2(q,t)$. Through the Siegert relation [90], $g^2(q,t)$ can be related to the first-order electric field correlation function:

$$g^2(q,t) = 1 + B|g^1(q,t)|^2 \quad (7)$$

where B ($\leq$1) is an instrumental parameter. For a population of particles with a certain size distribution, the decay of the correlation functions can be expressed by a single stretched exponential:

$$g^1(q,t) = \exp\left[-\left(\frac{t}{\tau_{se}}\right)^{\beta}\right] \quad (8)$$

where τ_{se} is the relaxation time characterizing the relaxation process, and β ($0 < \beta \leq 1$) characterizes the width of the distribution of the relaxation time. For monodisperse systems β can be set to equal 1.

For samples with a bimodal distribution of particles, e.g. solutions with unimers and micelles, or micelles and intermicellar aggregates, the correlation functions can be expressed by the sum of a single exponential and a stretched exponential [91]:

$$g^1(t) = A_f \exp\left[-\left(\frac{t}{\tau_f}\right)\right] + A_s \exp\left[-\left(\frac{t}{\tau_{se}}\right)^{\beta}\right] \quad (9)$$

where $A_f + A_s = 1$. A_f and A_s are the amplitudes of the fast and slow relaxation modes, respectively. τ_f and τ_{se} are the relaxation times characterizing the fast and slow relaxation. The fast mode is then be attributed to the diffusion of individual polymer coils, or small clusters of polymers, while the slow mode is attributed to intermicellar aggregates. The mean relaxation time for the slow mode is given by:

$$\tau_s = \left(\frac{\tau_{se}}{\beta}\right)\Gamma\left(\frac{1}{\beta}\right) \quad (10)$$

where $\Gamma(\beta^{-1})$ is the gamma functions of β^{-1}.

In dilute solutions of species, the relaxation mode is usually q^2 dependent. It exhibits diffusion behavior, where the relaxation time is inversely proportional to q^2 by [92]:

$$\tau = (Dq^2)^{-1} \quad (11)$$

From this, the R_h can be determined by the Stokes-Einstein relation (equation 6).

For complex systems with a bimodal relaxation process, the slow mode sometimes shows stronger q dependence than the diffusive mode. In these cases, large asymmetric clusters of, e.g., intermicellar aggregates may be present. Here, $qL \gg 1$ and it is no longer the global dimension that is probed, but the internal dynamics of the larger aggregates. Stokes-Einstein can thus not be used in the determination of R_h for these particles. However, other methods, such as static light scattering (SLS) are useful in these cases [93].

2.3.4 Small Angle Neutron Scattering

Small angle neutron scattering (SANS) is a powerful scattering technique to probe the local structures of colloids and polymers [87]. As the name indicates, SANS uses neutrons as the scattering source and measures at small scattering angles (< 10°). This provides a q-range of 0.005 $Å^{-1}$ to 0.8 $Å^{-1}$, corresponding to a length scale of 1 Å to 20 nm.

A great advantage with SANS over other scattering methods, is its sensitivity to the molecular composition [87]. As neutrons are elastically scattered by the atomic nuclei, different elements have different scattering lengths (how much they scatter the neutrons). ^1H and ^2H (hydrogen and deuterium) are good examples of this. Hydrogen has a scattering length of $-3.74 \cdot 10^{-5}$ Å, while deuterium has a scattering length of $6.67 \cdot 10^{-5}$ Å (the positive value of deuterium indicates a repulsive interaction potential). Thus, by replacing hydrogen with deuterium the scattering lengths of the solution components can be varied. This gives rise to the contrast variation technique, which enables SANS to not only see the global structure of the particles, but also probe their local structure, e.g. the size and composition of the core and shell in core-shell particles.

From a SANS measurement, the obtained scattered intensity, $I(q)$, can be analyzed in two different ways. The first method is to directly plot $I(q)$ vs q. If the plot has a plateau at low q-values (see Figure 11), the Guinier regime is observed. A Guinier plot can then be

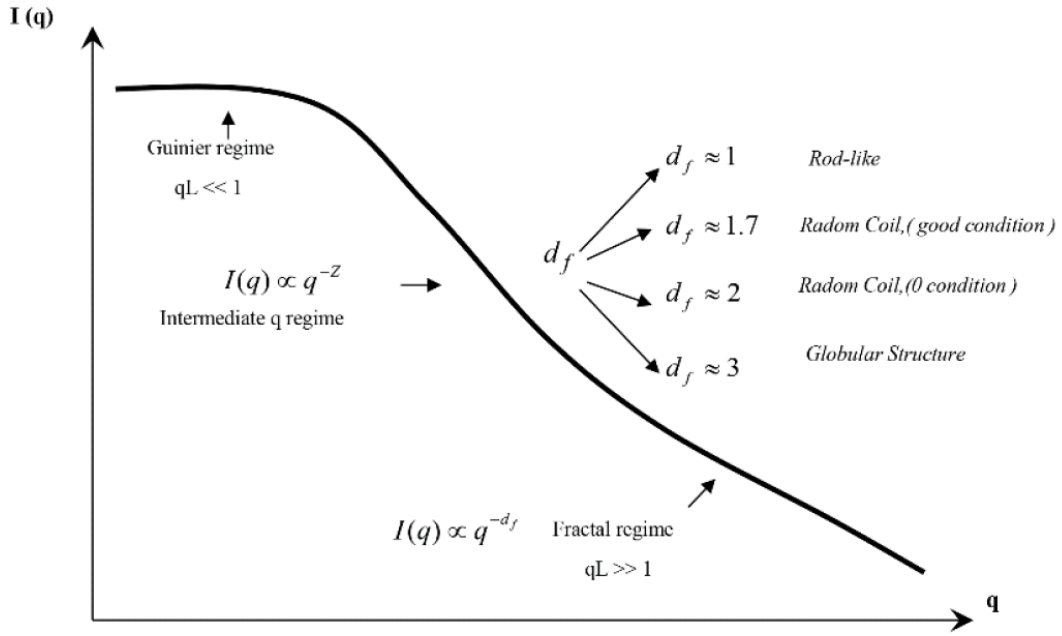

Figure 11. Schematic illustration of the SANS scattering intensity over an extended q-range. Picture borrowed from the thesis of B. Claro [94].

constructed with Ln[I(q)] vs q^2. From the slope of this curve, global information such as the particles' size (expressed in radius of gyration, R_g) can be obtained. If the curve displays a q dependence at high q-values, the fractal regime can be observed. Here a Porod plot of Log(I) vs Log(q) provides information about the fractal dimension, d_f, of the particles. This describes their local structure [87].

Another, more detailed method, is to fit the obtained data with precise models. The scattered intensity, $I(q)$, can be expressed as [95]:

$$I(q) = \frac{N}{V}(\rho_1 - \rho_2)^2 V_p^2 \cdot P(q) \cdot S(q) \qquad (12)$$

where N is the aggregation number, V is the scattering volume, V_p is the volume of the particle, and ρ_1 and ρ_2 are the scattering length densities of the particle and solvent, respectively. $P(q)$ is the form factor, which describes intraparticle correlations, and $S(q)$ is the structure factor, which describes interparticle correlations. For dilute systems, interparticle correlation is frequently neglected and the structure factor can be set to $S(q) = 1$. Since the form factor contains information about the size and shape of the scattering objects, it can be

modelled with different analytical expressions (describing geometric shapes such as e.g. spheres or cylinders) to investigate the shapes of the particles in solution.

For this study, the dilute systems were found be best fit with individual linear polymer chains, spherical core-shell particles, and elongated cylindrical core-shell particles. The form factor of these shapes are described in the Appendix.

2.3.5 Rheology

Rheology is the study of how a material flows or deforms as a function of force, time and spatial orientation. The two principal quantities measured in rheology are stress, which is the amount of force applied to a given area of the sample, and strain, which is the degree of how much a material deforms. From these two parameters, an array of rheological properties can be derived [96, 97].

Materials can be characterized by how viscous or how elastic they are. An ideal viscous fluid responds to stress by completely deforming and flowing. The molecular arrangement it had before the application of the stress is then broken and will not be restored. Ideal elastic solids, on the other hand, also deform with applied stress. However, the minute the stress is removed the elastic solid returns to its initial shape. Most materials have both a viscous and an elastic feature, in other words, they are viscoelastic [98]. The viscoelastic response of a material is usually dependent on the time scale that is probed [99].

Small amplitude oscillatory shearing (SAOS) is a good method to probe the viscoelastic properties of a material [99]. During these tests, the viscoelastic properties of a material are probed by applying a sinusoidal strain deformation on the sample and measuring the resultant stress response. In practice, this is performed by placing a sample between two plates, where one is stationary and the other oscillates with a frequency of, ω. The frequency (ω) is given in units of radians per second, and thus determines what time scales are probed. A typical rheometry setup is illustrated in Figure 12a.

One advantage with SAOS measurements is their gentle probation of the material. As the name indicates, small strain amplitudes are used during the study. The use of small strain amplitudes ensures that the structure of the material doesn’t break. The area within which the applied strain doesn’t break the material’s structure, is called the linear viscoelastic (LVE) regime. This can be determined by performing an amplitude sweep.

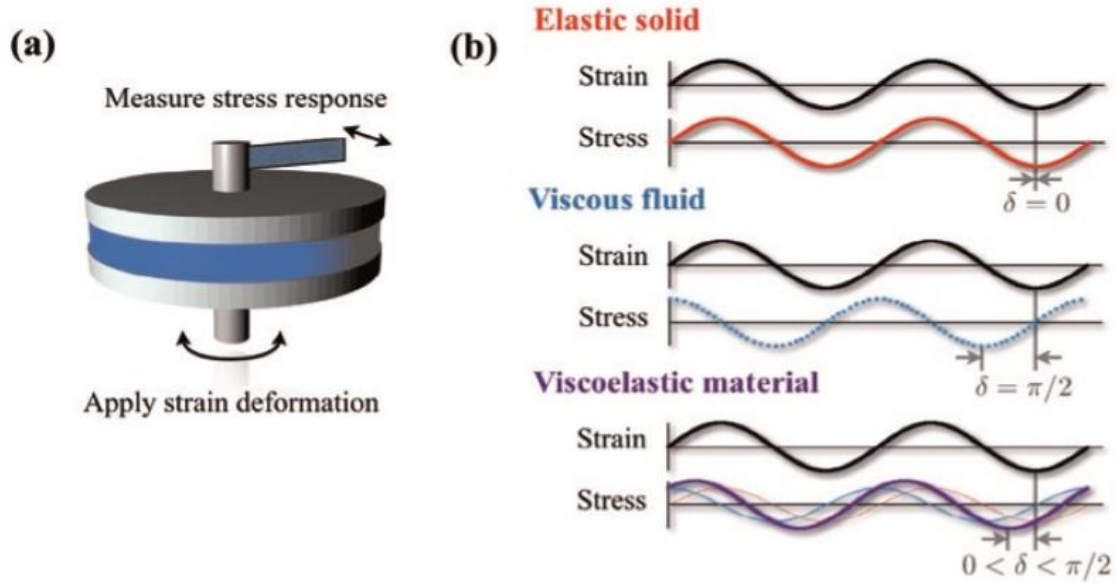

Figure 12. Schematic illustration of a) usual rheology instrument setup and b) the phase lag, tan δ, of the stress response of different materials. Picture borrowed from Weitz et al [100].

The sinusoidal strain, γ, applied on the sample can be expressed as:

$$\gamma = \gamma_0 sin\omega t \tag{13}$$

where γ_0 is a small enough strain amplitude that doesn't disrupt the structure of the material.

The linear response of the material in terms of stress can be written as:

$$\sigma = \sigma_0 \sin(\omega t + \delta) \tag{14}$$

where δ is the phase lag of the measured stress.

For an ideal elastic solid sample, the measured stress is in phase with the applied strain. For purely viscous fluids, the applied strain and the measured stress are out of phase with a phase angle of $\delta = \pi/2$. For viscoelastic materials, a phase lag between that of an ideal elastic solid and a viscous fluid is observed. The different phase lags are illustrated in Figure 12b.

The viscoelastic properties of the material can be characterized by the storage modulus, G', and the loss modulus, G'', which describe the solid-like and fluid-like contributions to the measured stress, respectively. The linear stress response of a viscoelastic material is then given by [99]:

$$\sigma = \gamma_0 [G'(\omega) \sin(\omega t) + G''(\omega) \cos(\omega t)] \tag{15}$$

The complex modulus, G^*, is:

$$G^*(\omega) \equiv G'(\omega) + iG''(\omega) \tag{16}$$

where i is $\sqrt{-1}$. The complex viscosity, η^*, is then given by:

$$\eta^*(\omega) \equiv \frac{G^*(\omega)}{i\omega} \tag{17}$$

How solid-like versus how fluid-like a material is can be described by the loss tangent:

$$\tan\delta = \frac{G''}{G'} \tag{18}$$

where $\tan\delta \gg 1$ for liquid-like materials and $\ll 1$ for solid-like materials.

Gel Point

For polymer systems exhibiting a sol-gel transition, rheology is a good method to characterize the exact temperature at which this occurs, also called the gel point. In 1986, Winter and Chambon found that the dynamic moduli of polymer systems follow a power law behavior at the gel point [101]:

$$G'(\omega) \sim G''(\omega) \sim \omega^n \tag{19}$$

where n ($0 < n < 1$) is the relaxation exponent. Furthermore, they observed that at the gel point, $\tan\delta$ becomes independent of frequency and is given by:

$$\tan\delta\,(\omega) = \frac{G''(\omega)}{G'(\omega)} = \tan\left(\frac{n\pi}{2}\right) \tag{20}$$

By plotting $\tan\delta$ obtained from different frequencies against temperature, the gel point can then be determined as the point at which the $\tan\delta$ curves collapse on each other (Figure 13).

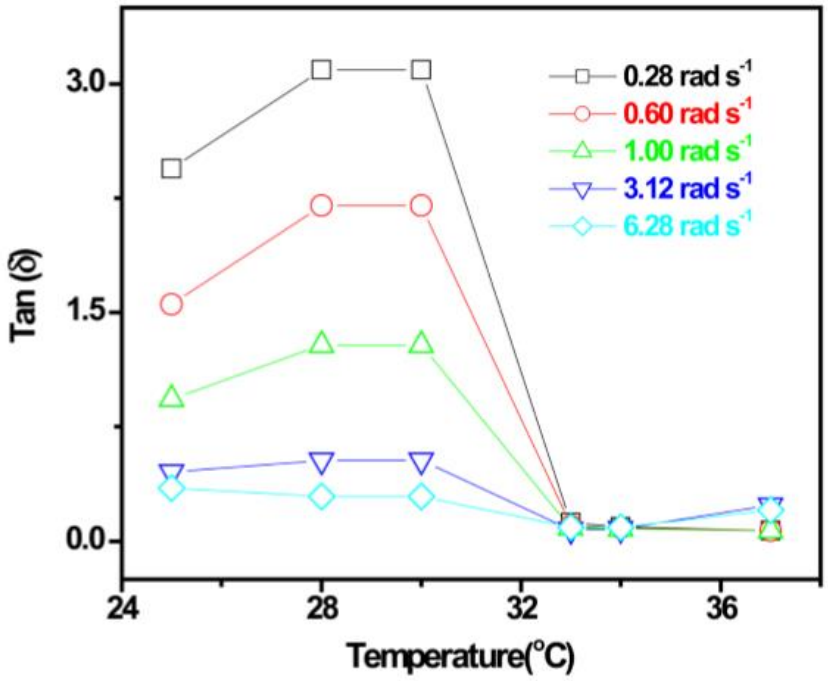

Figure 13. Gel point determination through observation of frequency independent tan δ. Picture borrowed from Zhou et al [102].

3 Experimental Section

3.1 Materials

Pluronic F127 (poly(ethylene oxide)-poly(propylene)-poly(ethylene oxide), PEO_{96}-PPO_{67}-PEO_{96}) was obtained from Sigma-Aldrich and used without further purification.

3.2 Synthesis of Polymer

In this study, PCL modified F127 block copolymers were investigated. These polymers were synthesized with two different strand lengths of PCL (n = 5 and 11) by Dr. Kaizheng Zhu, through a ring opening polymerization (ROP). The synthetic route is illustrated in Figure 14. In Table 1, the ratios and molecular weights of the synthesized polymers are presented.

For ease of identification, the PCL modified copolymers will from now be abbreviated as PCL(5) and PCL(11), respectively.

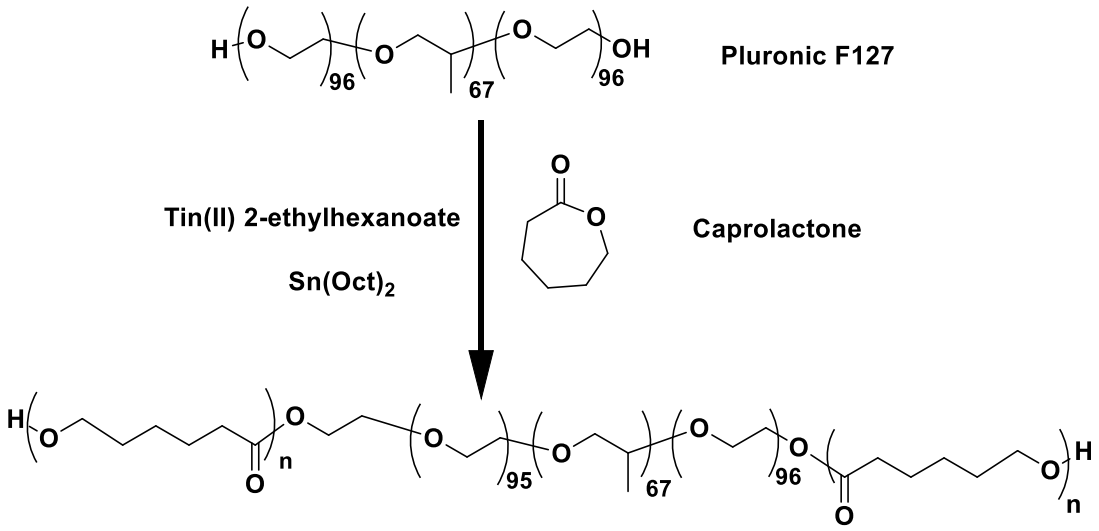

Figure 14. Synthetic scheme of Pluronic/PCL copolymers, with n repeating units of PCL.

Table 1. Physical parameters of the synthesized PCL-Pluronic-PCL Copolymers.

Polymer	CL/ F127	M_n (NMR)	M_w/M_n (GPC)	PDI
F127			13200/12600*	1.05
PCL(5)	10/1	13740 (570-12600-570)	16100/14100	1.14
PCL(11)	22/1	15110 (1250-12600-1250)	17700/15500	1.15

**Data measured by the AFFFF instrument in 0.01 N NaCl at 25°C.*

3.3 Sample Preparation

All samples were prepared by weighing a proper amount of polymer, based on the desired concentration, and dissolving it in Milli-Q type I water. To fasten the dissolution process and to obtain homogeneous solutions, the samples were stirred in a cold ice-bath for 2 hours with a magnetic stirrer. Afterward, they were kept in a refrigerator for 24 hours. All samples were prepared this way, with the exception of SANS samples, where deuterium oxide (D_2O, obtained from IFE, Kjeller) was used as the solvent to increase contrast and reduce background scattering.

3.4 Tube Inverting Method

To construct phase diagrams for the three polymer systems, the tube inverting method was performed [103]. For each copolymer, several concentrations were prepared. For F127 and PCL(5), 10, 15, 20, 25, and 30 wt% were tested. For PCL(11), high concentrations were found to be insoluble. Thus, for this polymer the concentrations of 2.5, 5.0, 7.5, 10, 12.5, and 15 wt% were tested. 1 mL of each solution was transferred into small glass tubes. The tubes were kept in a water bath and heated from 5 to 85 °C. To save time, the samples were first heated relatively fast to reveal the approximate phase behaviors. The measurements were then repeated. However, at temperatures close to the gelation temperature, samples were allowed to equilibrate with the temperature for 10 min. The sol-gel transition temperature was

determined by a flow to non-flow criterion over 1 minute. The reproducibility was checked by heating a second batch of prepared samples.

3.5 Turbidimetry

Turbidity measurements were performed with a NK60-CPA cloud point analyzer from Phase Technology, Richmond, BC, Canada. With the help of a micropipette, 0.15 mL of sample was placed on top of a special glass plate. This glass plate has a thin metallic layer coating of very high reflectivity, making it a mirror. To avoid evaporation of the solvent at elevated temperatures, the surface of the sample was covered with 0.15 mL of highly transparent silicon oil. A Peltier plate ensures effective and accurate temperature control, providing a temperature range of -60 to +60 °C and a fast maximum heating rate of 30 °C /min. For this study, a temperature interval of 10 to 50 °C was measured, with a heating rate of 0.2 °C /min. All samples were heated and cooled twice. The turbidity obtained from the second heating was used in the analysis of the results. To ensure reproducibility, the measurements were performed at least twice.

For this study, several concentrations were studied. However, due to no CP appearing for neither F127 nor PCL(5) even at 20 wt%, only 0.5 wt% concentrations are presented.

3.6 Dynamic Light Scattering

DLS measurements were performed with an ALV/CGS-8F multi-detector goniometer system, with eight fiber-optical detection units, from ALV-GmbH., Langen, Germany. A laser beam (He-Ne source, $\lambda = 632.5$ nm) was focused on the sample through a temperature-controlled cylindrical quartz container, which is filled with a refractive index matching liquid (*cis*-decalin). The temperature is controlled with a heating/cooling circulator, providing a temperature control of ±0.01 °C. The intensity of the scattered light was measured simultaneously at eight scattering angles from 22 to 141°. To avoid dust, the samples were filtered in an atmosphere of filtered air through a 0.2 μm filter into precleaned NMR tubes (10 mm). A series of temperatures from 10 to 50 °C was measured. The samples were allowed to equilibrate with the temperature for 20 min before measurements. Three measurements were performed at each temperature, with a measuring time of 2 min.

3.7 Rheology

Oscillatory shear experiments were performed with an Anton Paar-Physica MCR 301 rheometer. Cone-plate geometry was used, either with a diameter of 75 mm and a cone angle of 1°, or a diameter of 25 mm and a cone angle of 4°. The smaller cone was used for higher concentration samples to reduce the amount of sample needed. The instrument is equipped with a Peltier plate, providing an effective temperature control (±0.05 °C). To avoid evaporation at elevated temperatures and extended times, a thin layer of low-viscosity silicone oil was applied on the free surface of the solutions. This low-viscosity oil does not affect the viscoelastic response of the sample. Before performing any experiments, the rheometer was calibrated with water and standard high-viscosity oil.

To ensure that the experiments were performed within the LVE regime, amplitude sweeps were performed. The strain was varied from 0.01 to 100 %, with a constant angular frequency of 1 rad s^{-1}. A strain of 0.1 % was chosen for all samples.

To investigate the viscoelastic properties of the polymer systems, frequency sweeps were performed. These were done at every degree from 10 to 40 °C. The angular frequency was varied from 0.1 to 100 rad s^{-1}, with a constant strain of 0.1 %. The measurements were started at high temperatures and frequencies to avoid drying of samples. The frequency sweeps were repeated three times at each degree, with a pause of 2 min in between (found to be sufficient for the structures to recover). At every degree, the samples were allowed to equilibrate with the temperature for 20 min. To check reproducibility, new samples were checked for every concentration.

3.8 Small Angle Neutron Scattering

The SANS experiments were carried out at the Institute for Energy Technology (IFE) in Kjeller. The data were collected at two different detector distances (1.0 and 3.4 m) as well as two different wavelengths (5.1 and 10.2 Å) in order to obtain the largest possible q-range.

Dilute (0.5 and 2.0 wt%) and semidilute (10 and 20 wt%) concentrations of the three polymer systems were measured. However, 20 wt% PCL(11) was not measured due to its insolubility. The solutions were filled in 2 mm Hellma quartz cuvettes. The measurements were performed at a series of temperatures from 10 to 70 °C. At each temperature, the samples were allowed

to equilibrate for 2 h. To check the reversibility of the temperature behavior, measurements were repeated at two selected cooling temperatures (30 and 20 °C) for the 2.0 wt% samples.

Corrections for transmission of each sample as well as for the background were done using standard procedure.

4 Results and Discussion

4.1 Dilute Solutions

In this section, the results from the dilute solutions will be presented and discussed.

4.1.1 Turbidity

As already mentioned in the Introduction, Pluronic F127 has a LCST behavior mainly due to PPO (PEO also dehydrates, but at much higher temperatures). It is expected that when attaching PCL blocks to F127, the LCST behavior will still be present in the modified copolymer. However, with the addition of more hydrophobic PCL blocks the LCST should exist at lower temperatures, since hydrophobic interactions should be more probable in these systems. In Figure 15, the temperature dependencies of the turbidity at 0.5 wt% polymer concentrations are shown.

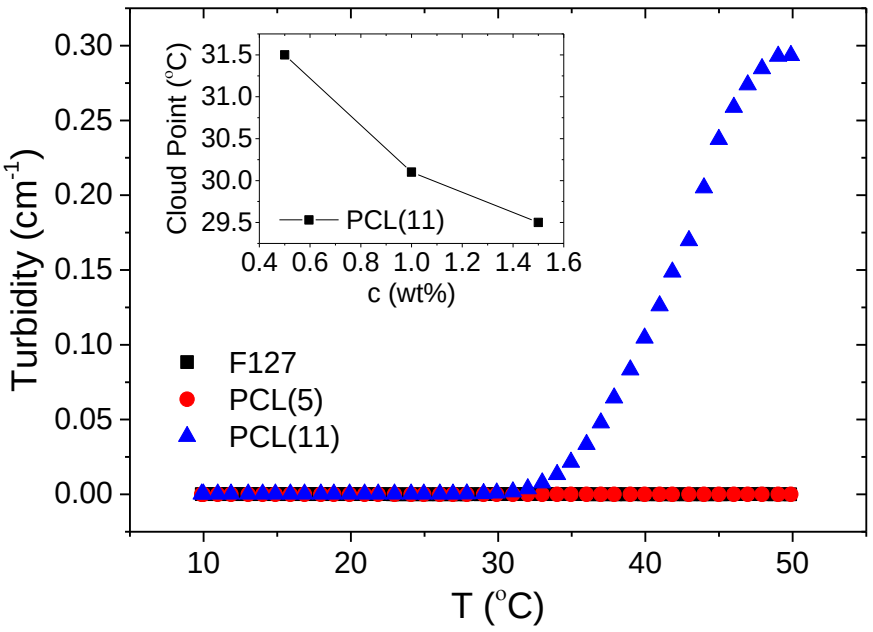

Figure 15. Calculated turbidity as a function of temperature for 0.5 wt% solutions of F127, PCL(5), and PCL(11), respectively. Every 60 points have been skipped to better observe each curve. Inset plot shows the concentration dependence of CP for PCL(11).

Looking first at the original polymer, F127, no increase in the turbidity is observed. From previous studies, it is already known that F127 has a high CP close to water's boiling point due to PEO's LCST behavior [104]. Since PEO is hydrophilic at elevated temperatures, the copolymers remain soluble during the heating. When PPO dehydrates, self-assembly into micelles occurs.

When attaching short PCL blocks to the copolymer, the turbidity curve of PCL(5) remains on the baseline in the measured temperature range. This shows that although hydrophobic PCL has been attached to the copolymer, F127's hydrophilic nature is maintained. This could be explained by the PCL blocks being short enough to effectively hide inside the micelle cores, leading to no increase in hydrophobic interactions and consequently no phase separation. Higher concentrations of PCL(5) (up to 20 wt%) were measured, with none of these showing any increase in the turbidity curve. However, from the phase diagram constructed, PCL(5) was found to phase separate around 80 °C, confirming that the PCL modified polymer has a lower LCST than F127.

Interestingly, when making the PCL blocks a little longer, a big difference is observed. In contrast to the other two copolymers, the turbidity curve of PCL(11) rises from the baseline already at about 30 °C. It continues to increase steadily up to 50 °C. Around this temperature, a significant dehydration of PCL probably leads to enhanced hydrophobic interactions and consequent growth of larger aggregates and phase separation. Thus, the effect of modifying the PCL length is clearly seen.

The concentration dependence of PCL(11) is shown in the inset plot in Figure 15. The CP is seen to decrease with increasing concentration. This is a known trend for LCST polymers, as higher concentrations increases the frequency and probability of polymers colliding and forming aggregates.

Dilute solutions of F127 are known to form individual micelles that are highly temperature stable. With a hydrophilic corona of PEO and PPO effectively hidden in the core, these micelles are not sticky and remain individual until PEO significantly dehydrates. PCL(5) most likely form flower-like micelles, with PCL effectively hidden in the core. However, for PCL(11) it may be difficult to effectively hide the PCL blocks inside the spherical micelle core due to their length. It was explained from the packing parameter that increasing the hydrophobic length can affect the morphology of the micelles. Thus, it could be that instead

of spherical micelles, PCL(11) forms elongated micelles that grow with temperature and eventually phase separate due to significant dehydration. However, this will be studied in more detail by SANS.

4.1.2 DLS

DLS measurements were performed on dilute 0.1 and 0.5 wt% polymer solutions to investigate the formation of aggregates and their sizes. To check the concentration dependence of F127 and PCL(5), 2.0 wt% solutions were measured as well. PCL(11) could not be measured at this concentration due to high turbidity.

In Figure 16, the normalized correlation functions (scattering angle of 90°) for 0.1 wt% F127, PCL(5), and PCL(11) at the indicated temperatures are presented. To take into account the trivial changes of solvent viscosity with temperature, the correlation functions have been plotted against the quantity tT/η_0.

A major difference that can be seen for the polymers directly from the correlation functions, is that for both F127 and PCL(5) correlation functions only appear from 40 °C and higher. Since the polymers are present in the system already from 10 °C, there should be diffusive processes present. However, since the solutions are very dilute and the polymers are most likely present as small individual unimers, the scattering of the light beam is low compared to that of larger scattering objects. This leads to low count rates and longer measuring times needed to get significant statistical data. The appearance of correlation functions at 40 °C can thus be explained by the presence of larger particles, as the measuring time (10 min) was held constant at all temperatures. At these high temperatures, the hydrophobic parts of the polymers have significantly dehydrated, leading to self-assembly of the polymers into micelles. Thus, the CMT behavior of these polymers is clearly displayed.

For PCL(11) correlation functions are present already from the lowest temperature measured (10 °C). In addition, the solutions only needed to be measured for 2 min in order to get good correlation functions. This demonstrates the better scattering of PCL(11) solutions, most likely due to enhanced self-assembly properties.

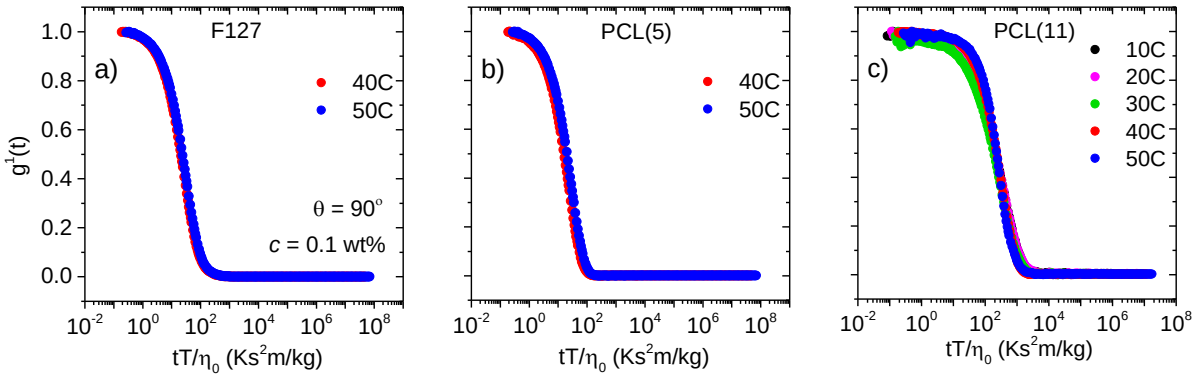

Figure 16. The first-order field correlation function (at a scattering angle of 90°) versus the quantity tT/η_0 for 0.1 wt% solutions of a) F127, b) PCL(5) and c) PCL(11) at the temperatures indicated.

Since the correlation functions are time-dependent, information about the size can be observed from them. It is seen that for F127 and PCL(5) the correlation functions decay at approximately the same time, indicating particles of similar sizes. However, for PCL(11) the decay of the correlation functions are shifted to slightly longer times than F127 and PCL(5). This shows that PCL(11) has longer relaxation times, indicating that the aggregates present in this system are larger than those in the other two polymer systems. A slight change with temperature is also observed for the polymers. However, this will be investigated in more detailed with model fittings of the correlation functions.

Before moving on to the analysis of the correlation functions, it is also interesting to observe if there is any concentration dependence for the polymers. Since F127 is known to form micelles that are effectively shielded from each other by the hydrophilic PEO corona, a concentration dependence is not expected for this polymer before a significant concentration increase. However, for the PCL modified polymers, it is interesting to see if a change of concentration leads to larger particles. This could then be attributed to the stickiness of PCL leading to enhanced connectivity between the entities.

For PCL(11) a concentration dependence has already been seen from turbidity measurements, with the formation of large particles occurring at lower temperatures with increasing concentration. Due to the turbidity of higher concentrations (c > 0.5 wt%) of PCL(11) and the resulting multiple-scattering problem, only the concentration dependence of F127 and PCL(5) will be probed by DLS.

In Figure 17, the concentration dependence of the correlation functions for F127 and PCL(5) at 40 °C has been plotted in the same graph to illustrate the differences. As expected, the correlation functions of F127 (black symbols) mostly overlap, indicating no concentration dependence from 0.1 wt% to 2.0 wt%. However, for PCL(5) (red symbols) it is seen that the 2.0 wt% solution is shifted to slightly longer times. Thus, a concentration dependence for PCL(5) is observed, with formation of larger aggregates at higher concentration due to the stickiness of PCL.

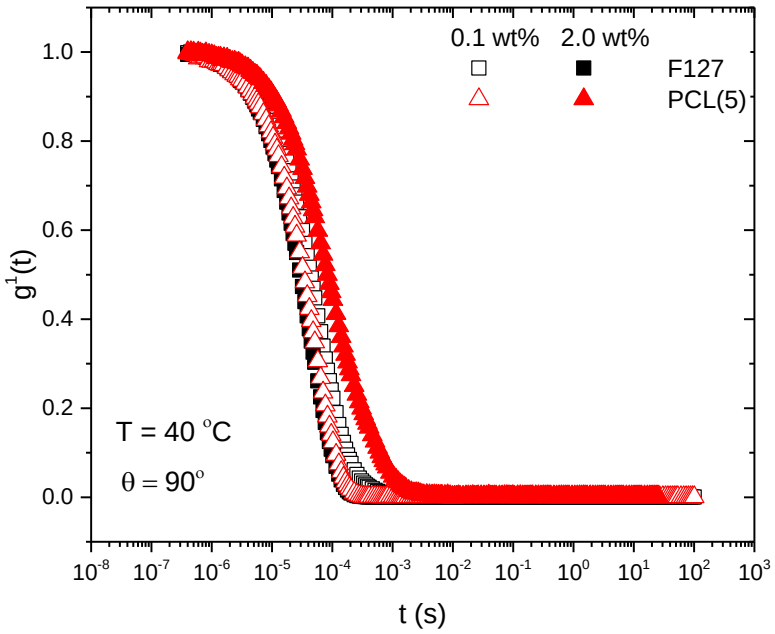

Figure 17. Time dependence of the first-order field correlation function (at a scattering angle of 90°) for 0.1 and 2.0 wt% of F127 and PCL(5).

Analysis of data

To get a more detailed picture of the population sizes in the polymer systems and their temperature dependence, the correlation functions have been fitted with the mathematical expressions described in chapter 2.4.3. Before fitting any data, the polymer systems were checked to be diffusive by plotting them against $t\,q^2$. If they collapsed on each other, the diffusive process was confirmed. Most of the solutions fulfilled this criterion. However, for 2.0 wt% PCL(5) and 0.1 wt% PCL(11), the functions were found to collapse on $t\,q^3$. For these systems interparticle interactions and internal motion is present ($qR_h > 1$). However, since it is

the characteristic growth of the aggregates with temperature that is interesting, the apparent hydrodynamic radius of these systems can still be investigated.

An illustration of the diffusive system checking and the fitting process is illustrated in Figure 18. The validity of the fittings were checked through residual plots.

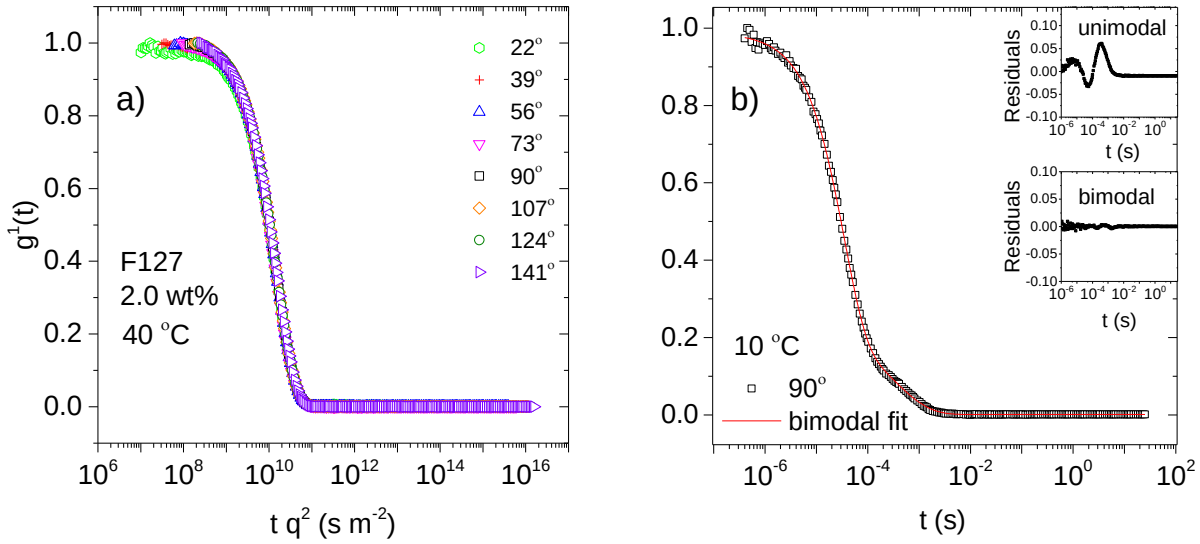

Figure 18. Illustration of the analysis of the correlation functions for 2.0 wt% F127 at the temperatures indicated. a) Shows the inspection of the collapse of the first-order field correlation functions against t q^2. b) Shows the bimodal exponential fit on the first-order field correlation function (scattering angle of 90°). Inset plots show the residual plots for the unimodal and the bimodal fit, respectively.

For 0.1 and 0.5 wt% F127 samples, good correlation functions appeared at 40 and 30 °C, respectively. These correlation functions were found to be fit with a single stretched exponential function (equation 8). For the 2.0 wt% sample, good correlation functions were present already at 10 °C. These functions were found to be expressed by the sum of a single exponential and a stretched exponential function (equation 9). Above 30 °C, the functions became unimodal. The transition from a bimodal correlation curve to a unimodal curve has been observed in other polymer systems [105, 106], and can be explained by a dominance of large particles in the correlation functions, due to consumption of unimers into micelles at elevated temperatures.

For the 0.1 wt% PCL(5), good correlation functions appeared from 40 °C and 50 °C. These were found to be best fit with a single exponential. For 0.5 wt% PCL(5), the functions were found to be bimodal from 10 °C up to 30 °C. At higher temperatures, the functions became unimodal, with a similar explanation as that of 2.0 wt% F127. For the 2.0 wt% PCL(5) solution, the functions were found to be bimodal throughout the whole temperature range. This concentration probably contains a mixture of micelles and intermicellar aggregates, where only a small fraction of the micelles takes part in the formation of intermicellar aggregates.

For the 0.1 wt% PCL(11) solution, the correlation functions were found to be bimodal below 30 °C and unimodal at higher temperatures. For 0.5 wt% PCL(11) the correlation functions were bimodal up to 30 °C. Above this temperature, it was not possible to fit the functions due to multiple scattering.

In Figure 19, the temperature dependencies of the apparent hydrodynamic radii, determined from the fast relaxation time ($R_{h,f}$) and the slow relaxation time ($R_{h,s}$), for the three polymers and concentrations indicated are shown. In Figure 19 a), $R_{h,f}$ is seen to cover a size range from about 2 nm to 14 nm for the three polymers. It is also seen that the temperature range reaches only 30 °C before $R_{h,f}$ disappears (with the exception of 2.0 wt% PCL(5)). This is probably due to consumption of the smaller species (e.g. unimers or micelles) into larger aggregates, resulting in a dominance of the larger species in the correlation functions.

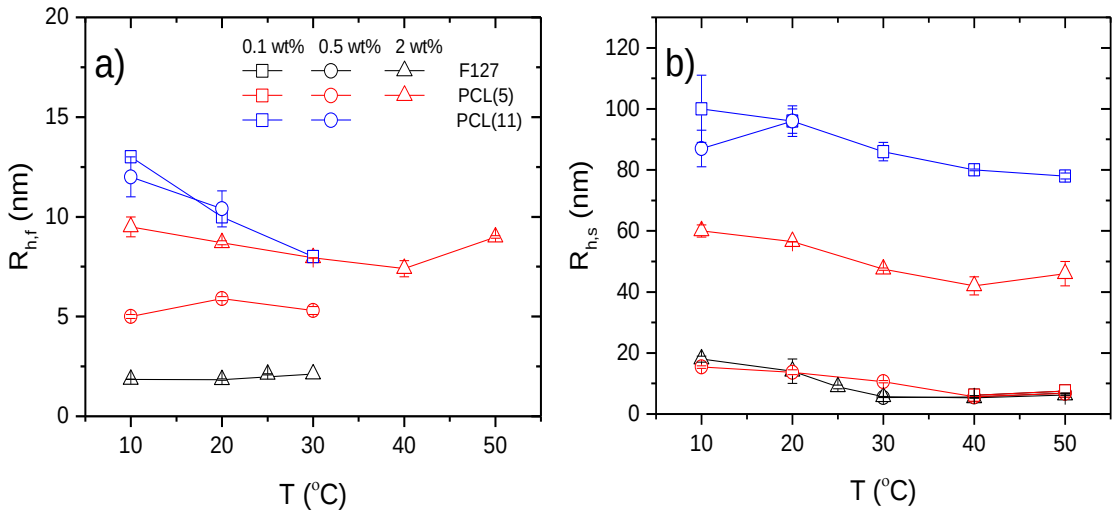

Figure 19. Temperature dependencies of a) $R_{h,f}$ and b) $R_{h,s}$ determined from the fast and slow relaxation time, respectively, for the polymers and concentrations indicated.

A clear trend that is observed in Figure 19 a) is that the attachment of PCL leads to larger aggregate sizes. The original F127 polymer (2.0 wt%), displays entities of about 2 nm from 10 to 30 °C. These are most likely individual unimers that float around in the solution. However, looking at 0.5 wt% PCL(5) (red symbols), entities of about 6 nm are seen. This size is in the range of micelles, indicating that PCL(5) self-assembles into micelles already at low temperatures. Thus, an enhanced micelle formation is seen for the PCL modified polymer. Furthermore, it is seen that a higher concentration of PCL(5) (2.0 wt%) leads to an $R_{h,f}$ of about 9-10 nm. This indicates a presence of intermicellar aggregates. Thus, it is seen that attaching a short PCL block to F127 both enhances its micelle formation, as well as its stickiness.

The largest sizes are seen for the polymer with the longest PCL blocks, PCL(11). For this polymer, even at very dilute solutions (0.1 wt%), species of about 12 nm are observed. Thus, it is seen that making the PCL block longer further enhances the self-assembly properties of the polymer and its stickiness.

It should also be noted that for PCL(11) and the 2.0 wt% PCL(5) systems, $R_{h,f}$ is seen to decrease with temperature. This indicates a compression of the entities with temperature, probably due to dehydration of the polymers at elevated temperatures.

In Figure 19 b), the apparent hydrodynamic radii determined from the slow relaxation time, $R_{h,s}$, is presented. Here the same trend of the aggregate sizes increasing with attachment of PCL is seen, although at a much larger scale. Whereas the species of F127 and $c < 0.5$ wt% PCL(5) solutions range from around 20 nm at low temperatures, to around 6-7 nm at high temperatures, PCL(11) solutions display sizes from around 90-100 nm at low temperatures to about 80 nm at high temperatures. It is thus clearly seen that PCL(11) indeed is much more sticky than the original polymer, and tend to gather into large intermicellar clusters.

For F127, the larger entities (2.0 wt%) at low temperatures are most likely highly swelled intermicellar aggregates, which compress at elevated temperatures due to dehydration of PPO. At 30 °C, $R_{h,s}$ is about 6-7 nm, which corresponds to the size of individual micelles. Similar sizes have been found by Attwood et al [107]. At these temperatures, a mixture of unimers, collapsed globular intermicellar aggregates and individual micelles probably exist. However, the unimers are not present in the correlation curves due to the dominance of the scattering

from micelles. It should also be noted that the different concentrations of F127 all overlap, indicating no concentration dependence on the micellar size.

For 0.5 wt% PCL(5), $R_{h,s}$ nearly overlaps with that of F127. A similar explanation of loosely connected intermicellar aggregates at low temperatures, and individual micelles at elevated temperatures can be given for this as well. At 2.0 wt%, PCL(5) has an $R_{h,s}$ of about 60 nm, which is significantly larger than that of F127. Here large intermicellar aggregates are present. Similarly to the lower concentration, 2.0 wt% PCL(5) also has an $R_{h,s}$ that decreases with temperature. Interestingly, it reaches a minimum at 40 °C, before slightly increasing at 50 °C. This indicates some kind of structural transition around this temperature.

For PCL(11), both 0.1 and 0.5 wt% solutions form large intermicellar aggregates of about 100 nm. The trend of $R_{h,s}$ decreasing with temperature is seen here too. However, in contrast to PCL(5), PCL(11) continues to decrease even above 40 °C.

The trend of F127/PCL systems shrinking with temperature has been observed by Kim et al [30]. They explained this by the dehydration of PPO at elevated temperatures. At low temperatures, the micellar corona of F127/PCL systems probably consist of relatively hydrophilic PPO and PEO. However, as the solution is heated PPO considerably dehydrates. As a result, the hydrophobic interactions between the PPO blocks and the PCL core increases, leading to a compression of the hydrophilic shell. It should be noted that although PEO has a high LCST, it has been found to start the dehydration process at lower temperatures [104]. Thus, the dehydration of PEO could also have an effect in the observed shrinking. However, since it is the global scale that is probed, it is difficult to draw a conclusion from these data only.

It is also interesting to observe how the stretched exponent β develops with increasing temperature, since this value describes the width of the size distributions in the solutions. In Figure 20, the temperature dependence of β for the three copolymers at the indicated concentrations are presented.

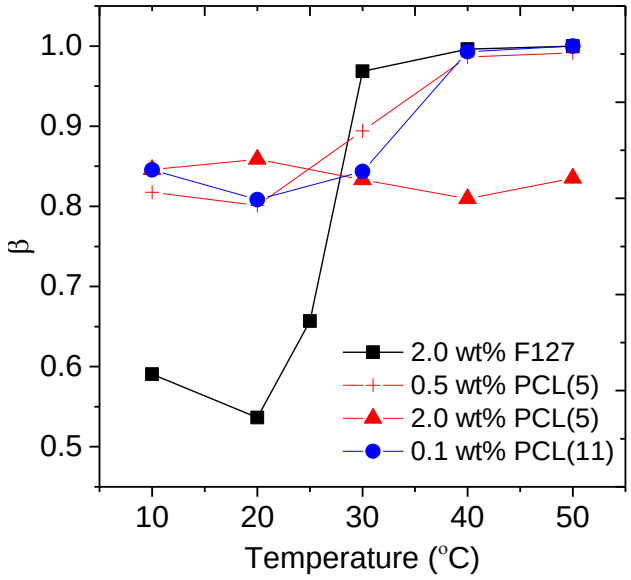

Figure 20. Temperature dependencies of the stretched exponent β for the polymers and concentrations indicated.

For both 2.0 wt% F127 and 0.5 wt% PCL(5) solutions, β approaches 1 as the samples are heated, indicating a narrow size distribution at elevated temperatures. This supports the earlier explanation of unimers being consumed into micelles, until eventually an abundance of monodisperse micelles are left in the solution. For 0.1 wt% PCL(11), β approaching 1 at elevated temperatures is also observed. Here the smaller intermicellar aggregates are probably consumed by the larger intermicellar clusters, due to significant dehydration above 30 °C.

For the 2.0 wt% PCL(5) solution, the trend of β approaching 1 is not observed. This is most likely due to the presence of a mixture of small species, e.g., unimers and micelles, and larger species i.e. intermicellar aggregates. The difference between PCL(5) and PCL(11), is that due to the shorter PCL length of PCL(5), the aggregates of this polymer don't experience the same significant dehydration that PCL(11) does. Thus, this mixture of small and large species is maintained throughout the temperature range. β therefore doesn't approach 1 at higher temperature.

From the results above, we can conclude that F127 systems consist of unimers and loose intermicellar aggregates below 30 °C. From 30 °C and higher, PPO is significantly dehydrated leading to the formation of monodisperse micelles with an R_h of about 6 nm.

Although the correlation functions reveal only one size population at elevated temperatures, it is likely that there exist a mixture of unimers and micelles. It is just not seen because of the domination of large micelles in the correlation functions.

For the PCL(5) system, we can conclude that at very dilute solutions (c < 0.5 wt%), a population of monodisperse individual micelles and intermicellar aggregates (around 20 nm) exist at low temperatures. The hydrophobic nature of PCL is displayed in the enhanced micelle formation, with PCL most likely composing the hydrophobic cores. At elevated temperatures, the loose intermicellar aggregates compress into globules the size of individual micelles, due to significant dehydration of PPO. At these temperatures, compressed globular aggregates, individual micelles, and unimers probably coexist. It is also interesting to note the almost equal sizes of F127 and PCL(5) micelles, indicating similar micelles formed in these systems.

For higher concentrations of PCL(5) (2.0 wt%) a population of small species (e.g., individual micelles and small intermicellar aggregates) and larger clusters of intermicellar aggregates are seen. This clearly displays the enhanced connectivity that the PCL modified polymer possesses. In contrast to the lower concentration solutions, 2.0 wt% PCL(5) doesn't become monodisperse at elevated temperatures. This can be explained by a continuous population of both small and large species even at elevated temperatures due to the hydrophilic nature that the polymer maintains.

For PCL(11), the significant role of PCL in micellar and intermicellar aggregation of F127 is well displayed. For these systems, a population of large intermicellar clusters exist even in very dilute systems (c < 0.5 wt%). This shows that making the PCL block a little longer drastically enhances the connectivity of these polymers.

4.1.3 SANS

As we have now seen, these three systems have very interesting self-assembling properties. It is now interesting to probe the actual structures of the aggregates formed. For this, SANS measurements have been performed. 0.5 and 2.0 wt% solutions have been measured for all three systems. In Figure 21, the SANS scattering patterns for the polymer solutions are presented.

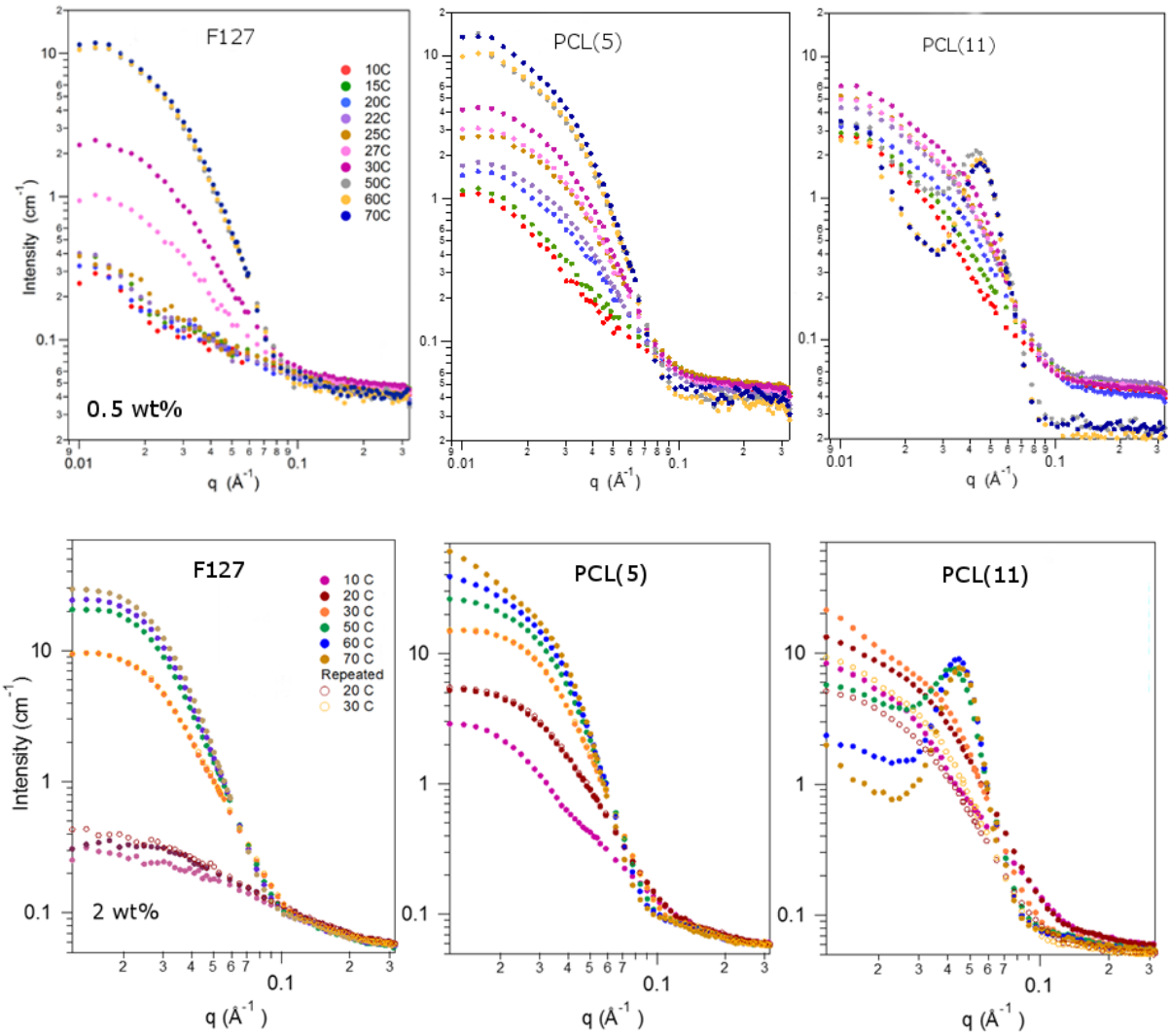

Figure 21. SANS patterns vs. temperature (10 °C to 70 °C) for 0.5 wt% and 2.0 wt% solutions of the polymers indicated. Repeated measurements were performed at 20 °C and 30 °C (open symbols) for the 2.0 wt% solutions.

The results reveal several interesting things. Looking first at the 0.5 wt% solutions, all three polymers have a plateau behavior in the low-*q* range. This shows scattering patterns typical of quite small micelles. Furthermore, a strong temperature dependence is revealed for all samples. In the case of F127, the micellar pattern appears from 27 °C and higher. The pattern then becomes systematically stronger with temperature, which indicates that the micelles are growing in size or that the population of micelles is growing. At 50 °C the pattern stabilizes and stays put up to 70 °C. This shows that the F127 micelles are highly stable with temperature, which is in line with previous work on F127 [63].

For the PCL modified polymers, micellar patterns are present already from the lowest temperature measured (10 °C). For PCL(5), a similar growth of the scattering intensity as for F127 is observed. The micellar pattern remains strong up to 70 °C, showing highly temperature stable micelles. However, for PCL(11) a drastic change in the scattering pattern occurs at 50 °C. Here a correlation peak appears, while at the same time the signal drops at high q. This indicates a strong ordering taking place, possibly due to significant local dehydration and subsequent aggregation. From the peak position, the ordering distance can be calculated through $d = 2\pi/q$. At 50 °C, the ordering distance is about 150 Å, while at 70 °C it is about 140 Å, showing increased dehydration with temperature. From turbidity measurements, a CP was found for PCL(11) at 30 °C. These results thus support each other.

Another difference observed for the two PCL modified polymers, is that the scattering intensity for PCL(11) at low temperatures is higher than the equivalent ones for PCL(5). This indicates that a longer PCL block enhances the micelle formation, with more or larger micelles present.

For the 2.0 wt% solutions, scattering patterns typical of interacting micelles are obtained for all three solutions. For F127, these patterns appear from 30 °C and remains strong up to 70 °C, showing that these micelles are very temperature stable. For PCL(5), a growth of the signal at low q with temperature is observed. At 70 °C, a homogenous network seems to be formed. For PCL(11), an abrupt transition is observed at 50 °C with an appearance of a second correlation peak indicating strong dehydration. This was also seen for the 0.5 wt%.

Furthermore, upon cooling and reheating of the samples to 20 and 30 °C, it is seen that for F127 and PCL(5) the scattering patterns completely overlap with the first measurements. For these polymers, the self-assembly in this temperature range is thus fully thermoreversible. However, for PCL(11) the intensity of the scattering patterns upon reheating is lower. This indicates fewer particles in the sample upon reheating, which can be explained by the formation of macroaggregates at elevated temperatures leading to macroscopic phase separation. Thus, a long PCL length is shown to destabilize these systems at higher temperatures.

These observations correspond well with the turbidity and DLS measurements performed on the polymer systems. As was seen in DLS, no aggregation was observed for 0.5 wt% F127 before 30 °C. SANS thus confirms the CMT behavior observed for this concentration. Furthermore, scattering patterns with interacting micellar structures are obtained at 2.0 wt%, which is in good agreement with DLS data, where both F127 and PCL(5) were found to have intermicellar aggregates. For PCL(11), a CP of around 30 °C was found. The appearance of tightly packed clusters at 50 °C supports the theory of PCL(11) forming large intermicellar aggregates that eventually phase separate.

Modelling of data

Since the 0.5 wt% solutions show scattering patterns similar to individual (non-interacting) micelles, quantitative information can be extracted from these through model fits.

The F127 system could be well fit with a model of spherical micelles with attached Gaussian chains from 27 °C and higher. The radius of the core (R_c) was found to be 35.0 Å, while the radius of the shell (R_g) was 29.2 Å. At 25 °C, the scattering pattern was best fit with the linear chain model. These results are in good accordance with the DLS measurements, where aggregates with an R_h of around 6 nm were present from 30 °C and higher.

For the PCL(5) system, micellar patterns were developed already at low temperatures. However, the scattering pattern at 10 °C resembled slightly more that of a linear coil than fully developed micelles. From DLS, aggregates with sizes similar to micelles were observed. However, DLS is much more sensitive to larger aggregates than SANS, as the latter looks at the average size of the whole population. The reason why SANS sees only polymer chains, can then simply be due to the larger presence of unimers over micelles at this low temperature. From 27 °C and higher, the scattering patterns were nicely fit with the spherical micelle model. The core was found to be 45.1 Å at 30 °C, while the radius of the shell was found to be 29.4 Å. Thus, it is shown that PCL(5) is able to effectively pack the PCL blocks in the spherical micelle cores, forming flower like micelles that are similar to the ones formed by F127.

Another interesting feature that these two systems have in common is how the aggregation number (N) significantly increases with temperature. As more unimers enter the micelles, one

could expect the micelles to grow or change shape. However, both F127 and PCL(5) remain spherical micelles, with hardly any increase in the micellar core size. Thus, the hydrophobic blocks probably pack themselves more effectively with temperature, resulting in a more compact core.

The fittings done on the PCL(11) system are presented in Figure 22. These fittings reveal structures much different than those of F127 and PCL(5). At 10 °C, the micellar pattern could be best fit with a spherical model. R_c was found to be 59 Å, while R_g 35 Å. This equals a total radius of about 10 nm. From DLS, aggregates with an R_h of about 12 nm and 100 nm were found for this solution. However, it should be noted that SANS is not always able to see large particles/aggregates in the system. In addition, the sizes measured by SANS are usually smaller than those measured by DLS due to the effect of the hydration layer.

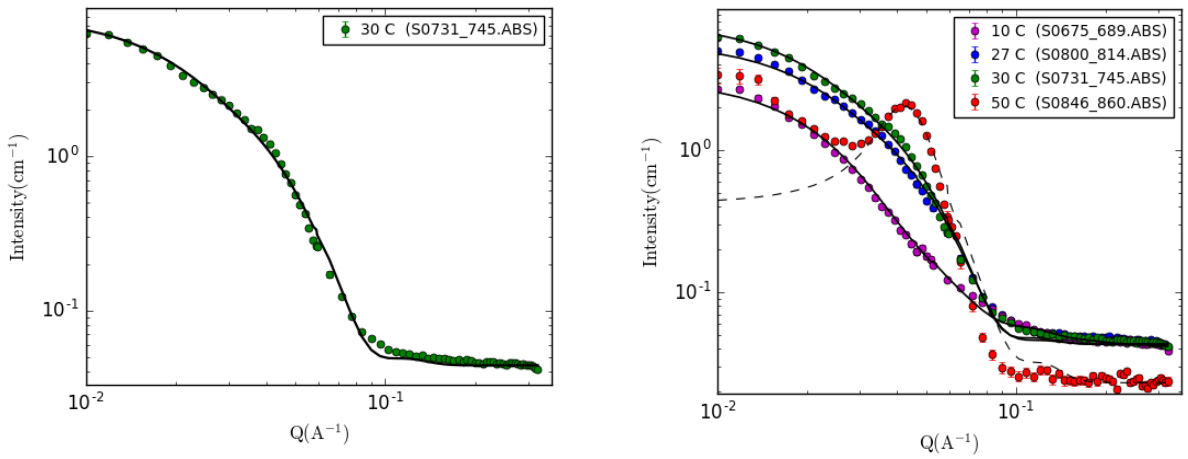

Figure 22. Left: The data for PCL(11) at 30 ºC with fit to a cylinder model. Right: Fit to four different temperatures, with the system changing from spherical micelles (10 ºC) to cylindrical micelles (27 and 30 ºC), and to highly dehydrated micelles with a correlation peak (50 ºC).

At higher temperatures, the pattern of PCL(11) changes to that of an asymmetric structure, which is revealed by the presence of two different slopes at low/medium *q*. At 27 °C, the pattern was best fit with a core-shell cylinder model with an axial rate of about 2.2. At 30 °C a cylinder with an axial ratio of 2.5 is revealed, showing that the cylinders grow in length with temperature, which can be explained by increased dehydration with temperature. At 50 °C it

was necessary to use an apparent volume fraction of 22% to explain the strength of this peak. This is much higher than the original sample concentraion (0.5%), showing clearly that we now have some regions that are strongly dehydrated, giving rise to more ordering and strong correlations, which was explained to be due to significant dehydration and tight packing of the entities.

The numerical results for the three polymer systems are shown in Table 2.

Table 2. Numerical results from the fitting of SANS data for 0.5 wt% F127, PCL(5), and PCL(11) solutions.

		F127			
T (°C)	R_g (Å) [1)]	R_c (Å)	R_g (Å) [2)]	N	Model
25	66				Linear coil
27		35.0	29.2	38	Sphere (core-corona)
30		37.6	"	61	"
50		45.6	"	139	"
		PCL(5)			
T (°C)	R_g (Å) [1)]	R_c (Å)	R_g (Å) [2)]	N	Model
10	115				Linear coil
27		42.4	27.2	49	Sphere (core-corona)
30		45.1	29.4	60	"
60		46.0	25.6	101	"
		PCL(11)			
T (°C)	R_g (Å) [1)]	R_c (Å)	R_g/d (Å) [2)]	N	Model
10		59.3	35.0	7	Sphere (core-corona)
27		31.6	16.6	-	Cylinder (core-shell)
30		35.4	14.7	-	"
50		~33	~14		Cylinder (core-shell) + S(q)[3]

R_g [1)] is the radius of gyration obtained from the linear coil fits, R_c is the core radius, R_g [2)] is the radius of gyration for the shell of the sphere model, d is the shell thickness of the cylinders, and N is the aggregation number.

From these model fits, the effect of attaching PCL to F127 and varying its length is clearly demonstrated. Due to the hydrophobicity of PCL, these chains arrange into the core of the aggregates, explaining why both PCL(5) and PCL(11) form micelles at low temperatures. However, in contrast to PCL(5), which forms temperature stable individual spherical flower-like micelles similar to those of F127, PCL(11) forms micelles that elongates with increasing temperature. This can be explained by a difficulty of arranging the hydrophobic core into a spherical shape due to steric hindrances at the core-corona interface. This consequently leads to a transition into elongated cylinder shapes. Due to the higher hydrophobicity of PCL(11), these polymers are also much less stable in aqueous solutions, leading to enhanced hydrophobic associations.

Now that the dilute solutions have been properly investigated, it is interesting to see how these systems behave in the semidilute region. The next part of the study will focus on this.

4.2 Semidilute Solutions

In this section, the results from the semidilute regime are presented and discussed.

4.2.1 Phase Diagram

The phase diagrams constructed for the three polymer systems are displayed in Figure 23.

For F127 a reversible sol-gel transition behavior is observed from c > 20 wt%. Below this concentration, the solutions are transparent, free-flowing liquids at all temperatures, with no observed phase separation. In the semidilute region (c > 20 wt%), the solutions go from being free-flowing liquids at low temperatures, to solid gels above the CGT. No phase separation is observed in the semidilute region either.

For PCL(5), a behavior similar to that of F127 is observed. It has a sol-gel transition from c > 20 wt%, and is a clear liquid below this temperature. However, there are some differences between F127 and PCL(5). The first difference is that the gel region of PCL(5) is smaller than that of F127. It is already known that the gelation of F127 is due to hydrophobic associations of PPO, which creates hydrophobic microdomains that form the gel network. However, in gels where hydrophobic associations are the main force behind the gelation, a delicate balance between network connectivity and swelling must be fulfilled. If swelling is dominant, a transient network may be formed, but no gel. If the hydrophobic forces on the other hand are dominating, the enhanced connectivity may lead to phase separation and no gel.

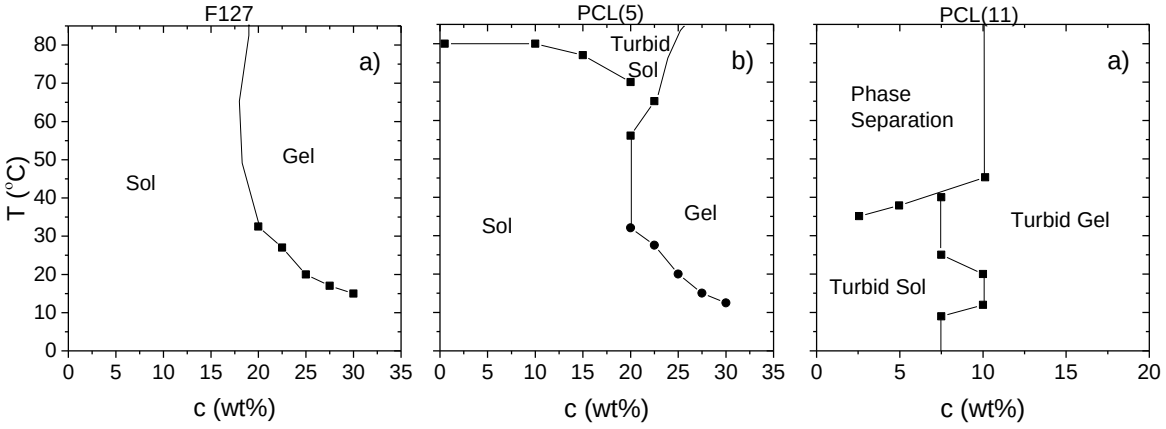

Figure 23. Phase diagrams for aqueous solutions of a) F127, b) PCL(5), and c) PCL(11). Lines have been added to better illustrate the different phases.

In light of this, the smaller gel region for PCL(5) may be explained by its higher hydrophobicity and the consequent domination of hydrophobic associations at elevated temperatures. In contrast to F127, where no phase observation is observed, PCL(5) solutions phase separate around 70-80 °C. At these elevated temperatures it may be difficult to keep PCL solubilized due to its increased hydrophobicity, in addition to the gradual dehydration of PEO.

Before moving on to the longer PCL modified F127, it should also be mentioned that opposed to semidilute F127 solutions, which were free-flowing liquids below the gel-transition temperature, PCL(5) display much more viscous solutions even in refrigerator temperature (around 4 °C). Its gel transition is much more gradual, becoming more and more viscous with increasing temperature until finally becoming a gel. This can be explained by the hydrophobic nature of the PCL blocks inhibiting free movement, as opposed to PPO which is only slightly hydrophobic allowing the chains to flow easily.

For PCL(11) a drastic difference in the phase behavior is observed. 20 wt% PCL(11) was found to be insoluble. The polymer needed to be diluted to 10 wt% to become a homogenous solution. Furthermore, it is seen that the solutions are turbid down to 2.5 wt%, indicating formation of large aggregates already at low concentrations, which has been confirmed by the dilute experiments (Turbidity, DLS, SANS). Similarly to PCL(5), the sol-gel transition for PCL(11) is not clear. In the refrigerator, 10 wt% PCL(11) is a solid gel. However, as it is slowly heated it becomes less and less viscous. Around 19 °C, it reaches its lowest viscosity, before turning into a solid gel as it is heated above 20 °C. A possible explanation for this behavior is that since gelation occurs through hydrogen bonding, as the sample is heated these bonds start to break leading to less viscosity. At even higher temperatures, gelation occurs through hydrophobic interactions. Around 44 °C, liquid exudes out of the gel and macroscopic phase separation occurs.

It was explained previously that a balance between swelling and connectivity is important for the gelation of F127. The smaller gel region for PCL(5) was explained due to its higher hydrophobicity. Similarly it is expected that PCL(11) forms gels with even smaller gel regions and at lower concentrations. These assumptions have been confirmed by the phase diagram.

4.2.2 Rheology

Rheology measurements were performed to see how PCL changes the viscoelastic properties of F127. To properly compare the three polymers, 10 wt% concentrations were first measured, as this was the highest concentration where PCL(11) showed a sol-gel transition. The temperature dependence of the complex viscosity, η^*, for the three different polymers are shown in Figure 24.

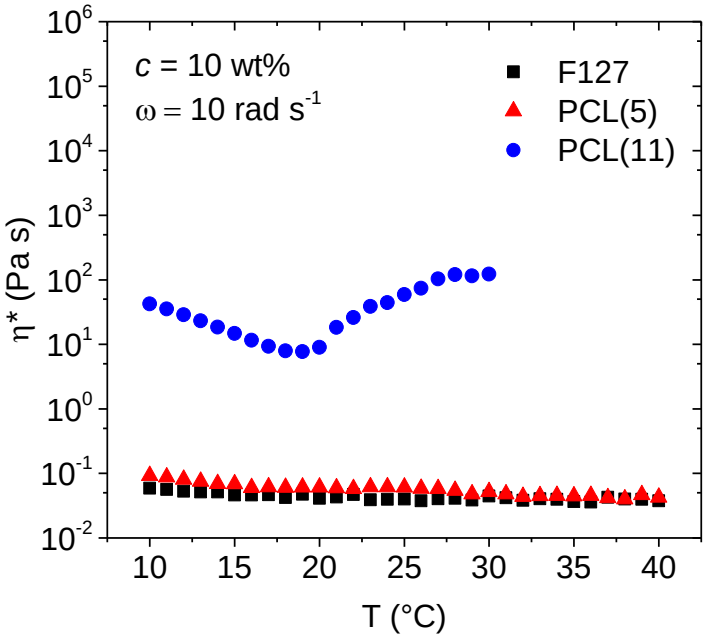

Figure 24. Temperature dependencies of the complex viscosity for the three polymer systems at a concentration of 10 wt% and a constant angular frequency of 10 rad s^{-1}.

For F127 and PCL(5) a low value of η^* (around 0.1 Pa s) is observed, which slightly decreases with increasing temperature. In these solutions no gel network is formed, and they consist of individual micelles or intermicellar aggregates that easily flow around. The slight decrease with temperature can probably be explained by a compaction of the micelles at elevated temperatures, subsequently making it easier to flow due to more space between the micelles. For PCL(11), however, higher η^* values (around 100 Pa s) are measured and a clear temperature dependence is observed. PCL(11) is seen to have a high η^* value at 10 °C, which decreases as the sample is heated. Around 19 °C it reaches a minimum. As it is further heated, it starts to increase up until 30 °C (due to phase separation above 30 °C, higher temperatures are not included). This indicates the formation of a network already at this low concentration,

which can be explained by its hydrophobic nature and subsequent promotion of hydrophobic associations.

It is now seen that a long PCL length drastically changes the viscoelastic properties of F127. However, it is also interesting to see how the shorter PCL length affects the gelation of F127. To do this, higher concentrations need to be measured. In Figure 25, the temperature dependence of η^* of semidilute PCL(5) and F127 solutions are presented.

For F127 a trend of η^* abruptly rising above a certain temperature is seen. This is associated with its sol-gel transition. With increasing concentration, the abrupt rise of η^* shifts to lower temperatures; from around 20 °C for 20 wt% to 10 °C for 30 wt%. This is expected as gel formation is enhanced at higher concentrations. Interestingly, the temperatures at which η^* rises, occur at lower temperatures than the gel point temperatures measured in the phase diagram. This have been observed earlier for Pluronic F68 by Bo Nyström et al [108], and was explained to be due to a gradual gelation that expands several degrees. The gelation point measured by the tube inverting method is not accurate, it just shows the trends of the polymer systems.

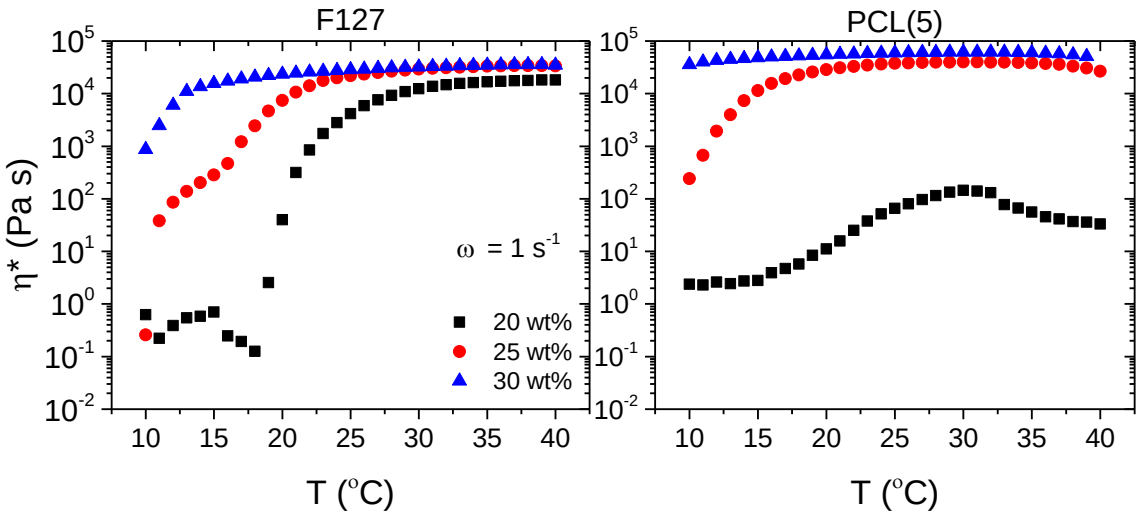

Figure 25. Temperature dependencies of the complex viscosity for a) F127 and b) PCL(5) at the concentrations indicated and a constant angular frequency of 1 rad s^{-1}.

For PCL(5) an increase of η^* with temperature is observed. However, in contrast to 20 wt% F127, which abruptly rose around 20 °C and reached a plateau around 10^4 Pa s, 20 wt% PCL(5) reaches a maximum at around 30 °C (about 100 Pa s), before slightly decreasing at higher temperatures. Here it seems that PCL(5) forms a weaker gel network than F127. A possible explanation to this could be that the short PCL chains are hidden inside the micelles. Upon heating, a contraction of the micelles occur due to PCL's hydrophobicity. Instead of a better network connectivity, this leads to the formation of a fragmented network and subsequent decrease of η^* at higher temperatures. A similar behavior has been seen in a gel forming PBO-PEO-PBO system by Castello et al [109]. They observed that the solid response of the system increased rapidly upon heating, but then decreased at even higher temperatures. They attributed this to a worsening in the solvent environment compressing the micellar core.

When increasing the concentration to 25 wt%, an abrupt increase of η^* around 10 °C is observed for PCL(5). In contrast to the 20 wt% solution, η^* reaches a plateau at around 20 °C and remains stable with temperature up until 35 °C. After this, a slight decrease of the curve is seen. At this concentration, there are probably enough polymers to form a proper gel network. It is interesting that the plateau of 25 wt% PCL(5) is almost equal to 25 wt% F127, indicating that these systems have gels of similar strength.

Further increasing the concentration to 30 wt%, it is seen that the sol-gel transition temperature for PCL(5) is gone, probably shifted to lower temperatures than measured. η^* is already at its plateau at 10 °C, and remains stable upon heating. A slight decrease above 35 °C, is observed for this concentration as well, possibly due to significant dehydration and contraction of the micelles. The reason for the disappearance of the sol-gel transition at this concentration is probably due to the stickiness of PCL. Here the polymer chains are significantly overlapping, enabling the PCL chains to stick together and form a gel network already at low temperatures. It should also be noted that the plateau of PCL(5) at this concentration is slightly higher than that of F127. This indicates a better connected network for PCL(5).

It is now seen that there are big differences between the short PCL length and the original F127 polymer as well. Higher concentrations are needed to form a proper network. In addition, the gelation property of PCL(5) is much more sensitive to concentration than F127.

From the temperature sweeps of η^*, a general picture of the gel transition for these polymers have been seen. However, it is also interesting to see the frequency sweeps of η^* degree by degree. In Figure 26, frequency sweeps of 25 wt% F127 and PCL(5), and 10 wt% PCL(11) at selected temperatures are presented.

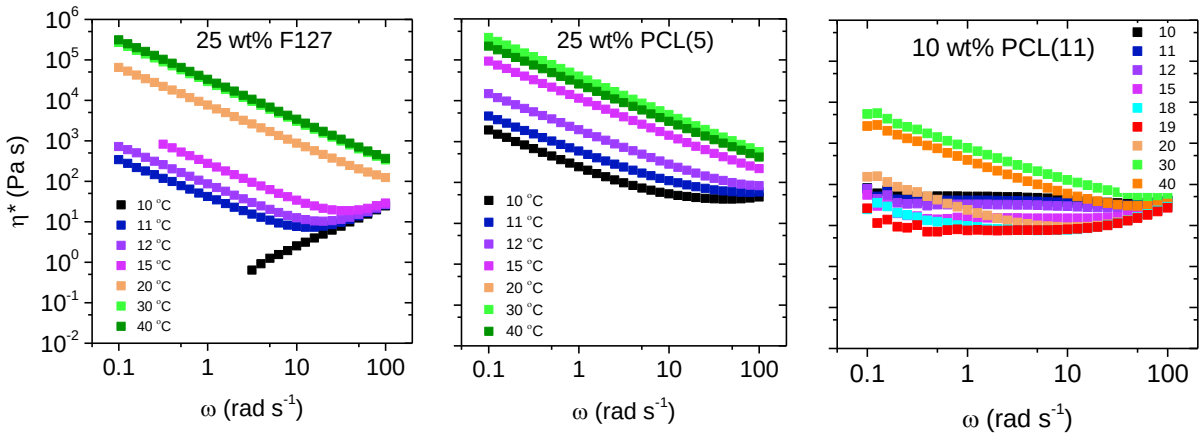

Figure 26. Frequency sweeps of η^* from 10 °C to 40 °C for the polymers, concentrations, and temperatures indicated. The plots have been given the same y-scales to better compare the systems.

For 25 wt% F127 at the lowest temperature, 10 °C, η^* is seen to increase with frequency. This is a characteristic of a liquid polymer solution where the chains become entangled at higher frequencies. This can be explained by a stretching of the chains at higher shear rates leading to an exposure of the hydrophobic parts and thus connectivity. From 11 °C and higher, η^* is seen to decrease with frequency. A power law $\eta^* \sim \omega^m$ can describe the curves, where *m*-values close to -1 indicate a solid-response. It is thus seen that between 10 and 11 °C, F127 goes from having a liquid-like response to a solid-like response. At higher temperatures, the *m*-value becomes steeper, indicating a stronger solid-like response.

For PCL(5), a much more solid-like response is seen already at 10 °C. With increasing temperature, η^* becomes steeper further enhancing its solid-like response. It is thus seen that this polymer has enhanced connectivity in the system compared to F127.

For PCL(11), η^* is nearly independent of the frequency below 15 °C, indicating a liquid-like behavior. The value of η^* is seen to decrease with temperature, indicating that the system is becoming less viscous. Between 19 and 20 °C, a solid-like response appears and becomes stronger with temperature. Despite the much lower concentration of PCL(11), this system also

possess solid-like features at elevated temperatures, clearly displaying the increased connectivity that a long PCL length provides.

Gel Point

Winter and Chambon's method of gel point determination has been carried out to investigate the gel point of the three polymers. In Figure 27, tan δ from different low frequencies have been plotted against temperature for 25 wt% F127 and PCL(5), and 10 wt% PCL(11). For F127 it is seen that tan δ decreases with temperature, indicating the transition from liquid-like to solid-like. Tan δ seems to become frequency independent at 12 °C, indicating a gel point around this temperature. Other studies has found a gel point at 14 °C for 25 wt% F127 [82]. For PCL(5), a gel point is found at approximately 13-14 °C, which is very similar to F127. Frequency sweeps of at these temperatures reveal parallel G′ and G″, indicating gel formation.

For PCL(11), tan δ begins at much higher values (around 10-25) than F127 and PCL(5). This indicates that PCL(11) is more liquid like than the two other polymers at low temperature. Tan δ seems to become frequency independent around 19-20 °C. However, when looking at G′ and G″, they are not parallel at these temperatures. It could possibly be explained by the gelation of this system being more gradual than the two other systems.

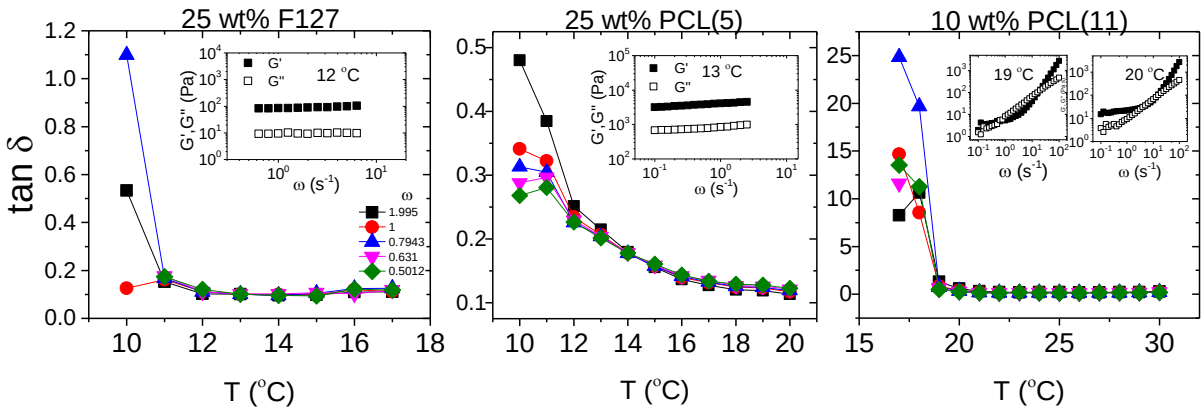

Figure 27. Multi-frequency tan δ versus temperature for the polymers and concentrations indicated. Inset plots show frequency sweeps of G′ and G″ at the indicated temperatures.

4.2.3 SANS

To see the details of what happens with the mesoscopic structures in the semidilute region, SANS measurements have been performed on 10 wt% polymer solutions and additional 20 wt% of F127 and PCL(5). In Figure 28, SANS data for 20 wt% solutions of F127 and PCL(5) are presented.

A trend that can immediately be seen for all three polymers is the presence of a correlation peak. This shows quite strong ordering of the systems already at 10 wt%. The peak lies at around q = 0.035 Å^{-1}, which indicates a characteristic length of 180 Å. For F127 the peak is absent at 10 and 15 °C, indicating no ordering at these temperatures. This is most likely due to PPO's hydrophilic nature in this temperature range, resulting in the polymer chains being well solved. However, as the solution is heated a gradual appearance of the peak comes at 20 °C. This becomes increasingly stronger with temperature. The peak can also be seen to shift slightly towards higher q-values, indicating a tightening of the ordered micelles with temperature. It was seen in the dilute solutions, that the micelle formation of F127 becomes more effective with temperature. At elevated temperatures there are thus more micelles, which results in less intermicellar space. Another interesting note is that the peaks move towards lower q-values above 30 °C. Some structural transition may occur between these temperatures.

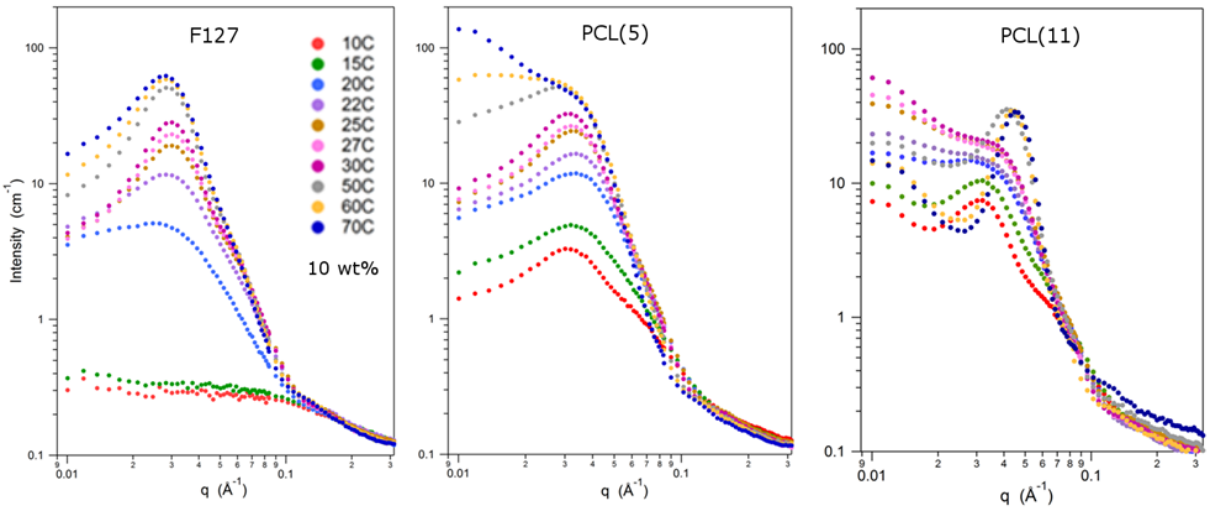

Figure 28. SANS patterns vs. temperature (10 °C to 70 °C) for 10 wt% samples.

For PCL(5) the correlation peak is present already at the lowest temperatures (10 and 15 °C). From the dilute solutions it was found that PCL(5) forms micelles already at low temperatures due to PCL's hydrophobic nature. Thus, it seems an ordering of these micelles occurs already at low temperatures. At 70 °C the peak seems to disappear, with a simultaneous increase of scattering signal at low *q*. This indicates a more homogenous network, which is possibly due to dehydration of the polymer. From the phase diagram, macroscopic phase separation was observed at 80 °C for 10 wt% PCL(5).

For PCL(11) the correlation peak is present at the lowest temperatures and up to the highest. It is seen that with increasing temperature, the peak continuously shifts to higher *q*-values, indicating a tighter ordering with temperature. From 50 °C and higher, the scattering at low *q* drops along with a more defined correlation peak, indicating the formation of smaller intermicellar clusters. The same behavior was seen for the dilute solutions (0.5 and 2 wt%).

In Figure 29, SANS data for 20 wt% solutions of F127 and PCL(5) are presented. Both systems show a clear correlation peak followed by a second correlation peak at slightly higher *q*. This indicates very strong ordering of the micelles in these systems. For F127, the peak is absent at 10 °C, but appears from 15 °C and above. For PCL(5), it is present at all temperatures.

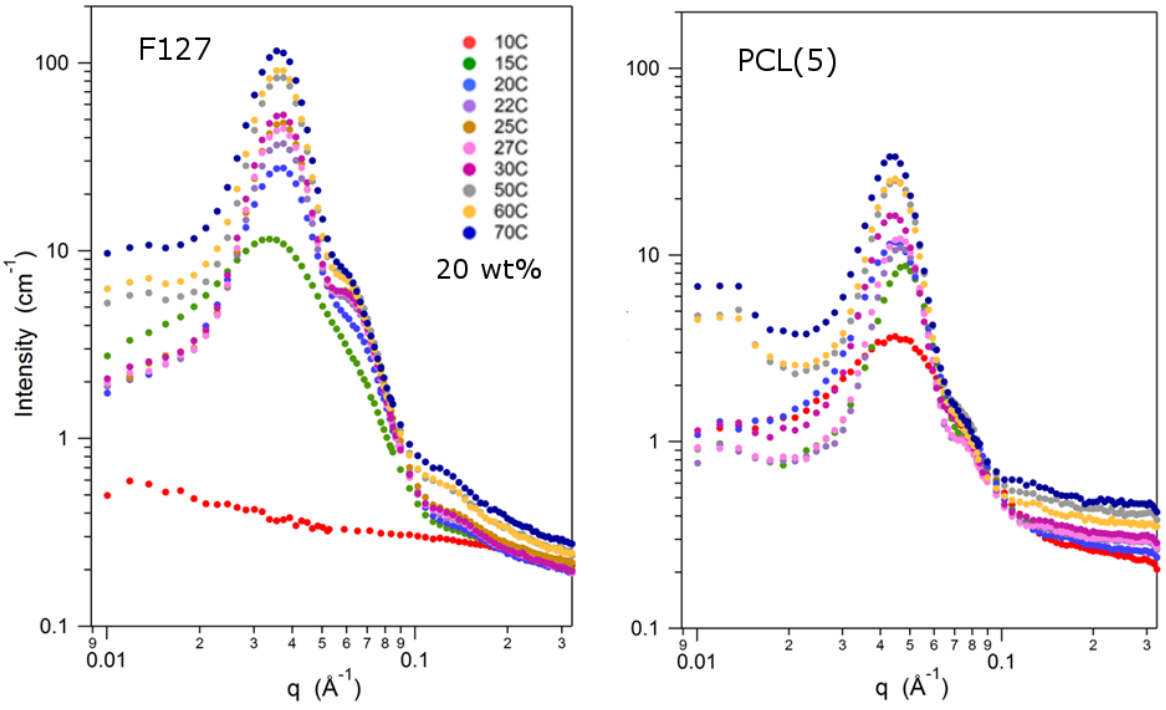

Figure 29. SANS patterns vs. temperature (10 °C to 70 °C) for 20 wt% samples.

The main differences between the two polymer systems is the higher intensity of the signal for F127, as well as its peaks being at slightly lower *q* than PCL(5). These differences show that the F127 system scatters more than PCL(5). In addition it is also less tightly packed than PCL(5).

From rheology it was seen that 20 wt% PCL(5) was poorer at forming a gel than F127. It was hypothesized that it could be because of compression of the micelle cores at elevated temperatures, which lead to a fragmented network. The lower scattering intensity and tighter packing of the PCL(5) system supports the suspicion of micellar compression.

To get a more exact picture of how the intermicellar distances differ for the three polymer systems, the characteristic length from each correlation peak has been calculated and plotted in Figure 30.

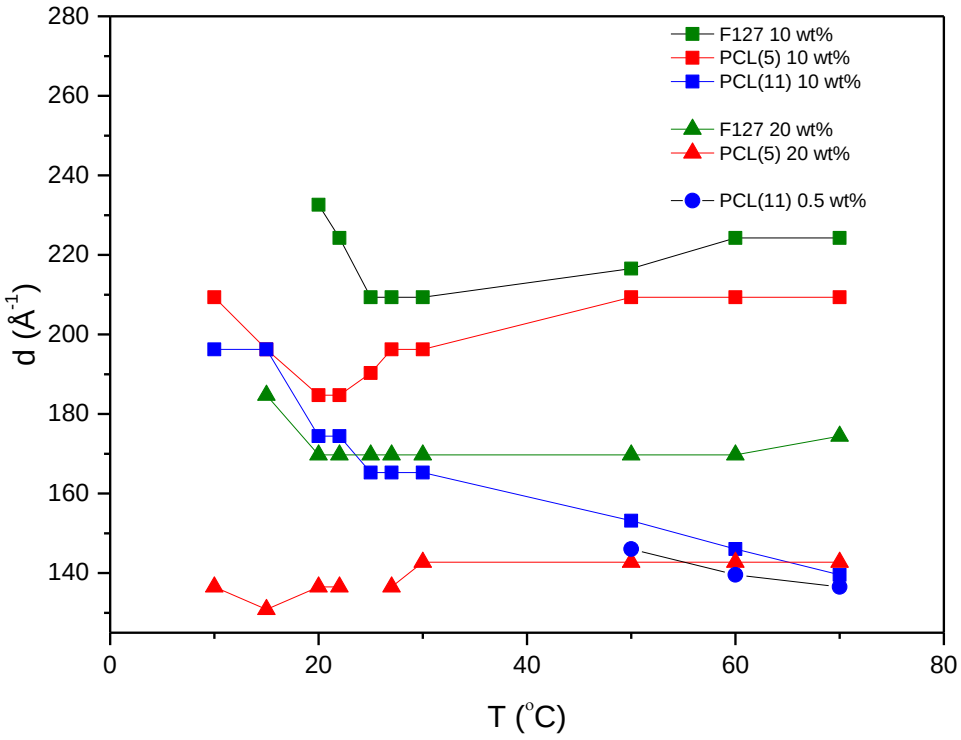

Figure 30. The intermicellar distance as extracted from the position of the correlation peak ($d = 2\pi/q$) for all samples and temperatures where a correlation peak could be identified.

From Figure 30, several interesting things can be observed. For all three 10 wt% polymer systems, the intermicellar distance is seen to decrease with temperature. This indicates a tighter ordering with temperature, which is probably due to dehydration of the polymers. Furthermore, it is seen that attaching PCL to F127 leads to a smaller intermicellar distance, where a longer PCL length gives the smallest distance. It is also seen that increasing the concentration of F127 and PCL(5) leads to less space between the micelles which is to be expected.

However, an interesting difference between the F127 and PCL(5) solutions compared to PCL(11), is the different trends these display with temperature. For F127 and PCL(5), a trend of the intermicellar distance decreasing with temperature before slightly increasing at even higher temperatures is seen. This indicates some structural transition for these polymers with temperature. In the case of 10 wt% F127, the intermicellar distance is seen to reach a minimum distance of 210 Å at 25 °C. This distance is kept up to 30 °C. At 40 °C, the distance increases to 216 Å, and continues to further increase up to 225 Å at 70 °C. For 10 wt% PCL(5), a minimum distance of 185 Å is reached at 20 °C. Interestingly, this increases to 195 Å at 27 °C, before reaching a maximum of 210 Å at 70 °C.

The intermicellar distance of 10 wt% PCL(11), however, continuously decreases with temperature. It starts with having a distance of about 196 Å at 10 °C. Then, as it is heated to 25 °C, it reaches an intermicellar distance of 165 Å. Upon further heating, it eventually compresses into a distance of 140 Å at 70 °C. The intermicellar distance of 0.5 wt% PCL(11) was also calculated and is seen to be almost equal to the 10 wt% PCL(11). Thus, it is shown that at elevated temperatures the intermicellar distance is independent of concentration. Here, significant local dehydration dominates leading to formation of tightly packed intermicellar clusters.

5 Conclusion

The main objective of this study was to investigate the different structural and dynamic properties of an amphiphilic PCL-F127-PCL pentablock copolymer, with the original F127 triblock copolymer as a reference. The influence of PCL was examined by having two different lengths of PCL covalently bound to F127.

From the investigation of the dilute region, both the PCL groups and the length of the PCL block were found to have a pronounced impact on both the self-assembly and structural properties of the polymer systems. Turbidity measurements revealed that a long PCL block drastically lowered the CP of the system. From DLS measurements, it was found that PCL greatly enhanced the micelle formation and intermicellar connectivity of these systems. SANS measurements disclosed that the micellar structures depended greatly on the length of the PCL block.

From the investigation of the semidilute region, a long PCL length was seen to drastically change both the macroscopic and mesoscopic behavior of the systems. The constructed phase diagram exposed a more gradual gel formation for the PCL modified polymers. Furthermore, the gel phase was shifted to significantly lower concentrations for the polymer with a long PCL length, which demonstrated the importance of the hydrophobic end-groups. From rheology experiments, it was found that a short PCL length lead to the formation of a poorer gel network. Higher concentrations were needed to form proper gels, while no significant increase in mechanical strength was observed. SANS measurements revealed a tighter ordering in the PCL modified systems.

In this study it has been shown that PCL-F127-PCL copolymers possess great tuning ability through the PCL blocks. Furthermore, these systems have a lower CMC and CMT than the original F127 copolymer, making them good candidates for drug delivery.

References

1. Kataoka, K., A. Harada, and Y. Nagasaki, *Block copolymer micelles for drug delivery: Design, characterization and biological significance.* Advanced Drug Delivery Reviews, 2001. **47**(1): p. 113-131.
2. Rösler, A., G.W. Vandermeulen, and H.-A. Klok, *Advanced drug delivery devices via self-assembly of amphiphilic block copolymers.* Advanced drug delivery reviews, 2012. **64**: p. 270-279.
3. Blanazs, A., S.P. Armes, and A.J. Ryan, *Self-assembled block copolymer aggregates: From micelles to vesicles and their biological applications.* Macromolecular Rapid Communications, 2009. **30**(4-5): p. 267-277.
4. Chiappetta, D.A. and A. Sosnik, *Poly(ethylene oxide)–poly(propylene oxide) block copolymer micelles as drug delivery agents: Improved hydrosolubility, stability and bioavailability of drugs.* European Journal of Pharmaceutics and Biopharmaceutics, 2007. **66**(3): p. 303-317.
5. Vonarbourg, A., C. Passirani, P. Saulnier, and J.-P. Benoit, *Parameters influencing the stealthiness of colloidal drug delivery systems.* Biomaterials, 2006. **27**(24): p. 4356-4373.
6. Klibanov, A.L., K. Maruyama, V.P. Torchilin, and L. Huang, *Amphipathic polyethyleneglycols effectively prolong the circulation time of liposomes.* FEBS Letters, 1990. **268**(1): p. 235-237.
7. Hoffman, A.S., *Hydrogels for biomedical applications.* Advanced Drug Delivery Reviews, 2012. **64, Supplement**: p. 18-23.
8. Hamidi, M., A. Azadi, and P. Rafiei, *Hydrogel nanoparticles in drug delivery.* Advanced Drug Delivery Reviews, 2008. **60**(15): p. 1638-1649.
9. Nie, S., W.L.W. Hsiao, W. Pan, and Z. Yang, *Thermoreversible pluronic(®) f127-based hydrogel containing liposomes for the controlled delivery of paclitaxel: In vitro drug release, cell cytotoxicity, and uptake studies.* International Journal of Nanomedicine, 2011. **6**: p. 151-166.
10. Yu, L. and J. Ding, *Injectable hydrogels as unique biomedical materials.* Chemical Society Reviews, 2008. **37**(8): p. 1473-1481.
11. Klouda, L., *Thermoresponsive hydrogels in biomedical applications: A seven-year update.* European Journal of Pharmaceutics and Biopharmaceutics, 2015. **97, Part B**: p. 338-349.
12. Fusco, S., A. Borzacchiello, and P.A. Netti, *Perspectives on: Peo-ppo-peo triblock copolymers and their biomedical applications.* Journal of Bioactive and Compatible Polymers, 2006. **21**(2): p. 149-164.
13. Batrakova, E.V. and A.V. Kabanov, *Pluronic block copolymers: Evolution of drug delivery concept from inert nanocarriers to biological response modifiers.* Journal of Controlled Release, 2008. **130**(2): p. 98-106.
14. Kabanov, A.V., E.V. Batrakova, and V.Y. Alakhov, *Pluronic® block copolymers as novel polymer therapeutics for drug and gene delivery.* Journal of controlled release, 2002. **82**(2): p. 189-212.
15. Alexandridis, P., J.F. Holzwarth, and T.A. Hatton, *Micellization of poly(ethylene oxide)-poly(propylene oxide)-poly(ethylene oxide) triblock copolymers in aqueous solutions: Thermodynamics of copolymer association.* Macromolecules, 1994. **27**(9): p. 2414-2425.
16. Alexandridis, P. and T. Alan Hatton, *Poly(ethylene oxide) · poly(propylene oxide) · poly(ethylene oxide) block copolymer surfactants in aqueous solutions and at interfaces: Thermodynamics, structure, dynamics, and modeling.* Colloids and Surfaces A: Physicochemical and Engineering Aspects, 1995. **96**(1): p. 1-46.
17. Mortensen, K. and J.S. Pedersen, *Structural study on the micelle formation of poly (ethylene oxide)-poly (propylene oxide)-poly (ethylene oxide) triblock copolymer in aqueous solution.* Macromolecules, 1993. **26**(4): p. 805-812.
18. Mortensen, K. and Y. Talmon, *Cryo-tem and sans microstructural study of pluronic polymer solutions.* Macromolecules, 1995. **28**(26): p. 8829-8834.

19. Wu, C., T. Liu, B. Chu, D.K. Schneider, and V. Graziano, *Characterization of the peo-ppo-peo triblock copolymer and its application as a separation medium in capillary electrophoresis.* Macromolecules, 1997. **30**(16): p. 4574-4583.
20. Prud'homme, R.K., G. Wu, and D.K. Schneider, *Structure and rheology studies of poly(oxyethylene−oxypropylene−oxyethylene) aqueous solution.* Langmuir, 1996. **12**(20): p. 4651-4659.
21. Lee, Y., H.J. Chung, S. Yeo, C.-H. Ahn, H. Lee, P.B. Messersmith, and T.G. Park, *Thermo-sensitive, injectable, and tissue adhesive sol-gel transition hyaluronic acid/pluronic composite hydrogels prepared from bio-inspired catechol-thiol reaction.* Soft Matter, 2010. **6**(5): p. 977-983.
22. Gong, C.Y., S. Shi, P.W. Dong, X.L. Zheng, S.Z. Fu, G. Guo, J.L. Yang, Y.Q. Wei, and Z.Y. Qian, *In vitro drug release behavior from a novel thermosensitive composite hydrogel based on pluronic f127 and poly(ethylene glycol)-poly(ε-caprolactone)-poly(ethylene glycol) copolymer.* BMC Biotechnology, 2009. **9**(1): p. 8.
23. Liu, Y., W.-L. Lu, J.-C. Wang, X. Zhang, H. Zhang, X.-Q. Wang, T.-Y. Zhou, and Q. Zhang, *Controlled delivery of recombinant hirudin based on thermo-sensitive pluronic® f127 hydrogel for subcutaneous administration: In vitro and in vivo characterization.* Journal of Controlled Release, 2007. **117**(3): p. 387-395.
24. Wu, C.-J., A.K. Gaharwar, B.K. Chan, and G. Schmidt, *Mechanically tough pluronic f127/laponite nanocomposite hydrogels from covalently and physically cross-linked networks.* Macromolecules, 2011. **44**(20): p. 8215-8224.
25. Chun, K.W., J.B. Lee, S.H. Kim, and T.G. Park, *Controlled release of plasmid DNA from photo-cross-linked pluronic hydrogels.* Biomaterials, 2005. **26**(16): p. 3319-3326.
26. Ma, W.-D., H. Xu, C. Wang, S.-F. Nie, and W.-S. Pan, *Pluronic f127-g-poly(acrylic acid) copolymers as in situ gelling vehicle for ophthalmic drug delivery system.* International Journal of Pharmaceutics, 2008. **350**(1–2): p. 247-256.
27. Goldberg, D., *A review of the biodegradability and utility of poly(caprolactone).* Journal of environmental polymer degradation, 1995. **3**(2): p. 61-67.
28. Dash, T.K. and V.B. Konkimalla, *Poly-ϵ-caprolactone based formulations for drug delivery and tissue engineering: A review.* Journal of Controlled Release, 2012. **158**(1): p. 15-33.
29. Zhou, Q., Z. Zhang, T. Chen, X. Guo, and S. Zhou, *Preparation and characterization of thermosensitive pluronic f127-b-poly(ε-caprolactone) mixed micelles.* Colloids and Surfaces B: Biointerfaces, 2011. **86**(1): p. 45-57.
30. Kim, S.Y., J.C. Ha, and Y.M. Lee, *Poly(ethylene oxide)-poly(propylene oxide)-poly(ethylene oxide)/poly(ϵ-caprolactone) (pcl) amphiphilic block copolymeric nanospheres: Ii. Thermo-responsive drug release behaviors.* Journal of Controlled Release, 2000. **65**(3): p. 345-358.
31. Oh, S.H., T.H. Kim, S.Y. Chun, E.K. Park, and J.H. Lee, *Enhanced guided bone regeneration by asymmetrically porous pcl/pluronic f127 membrane and ultrasound stimulation.* Journal of Biomaterials Science, Polymer Edition, 2012. **23**(13): p. 1673-1686.
32. Kwon, S.K., H.-B. Kim, J.-J. Song, C.G. Cho, S.-W. Park, J.-S. Choi, J. Ryu, S.H. Oh, and J.H. Lee, *Vocal fold augmentation with injectable polycaprolactone microspheres/pluronic f127 hydrogel: Long-term in vivo study for the treatment of glottal insufficiency.* PLOS ONE, 2014. **9**(1): p. e85512.
33. Fuentes, I., B. Blanco-Fernandez, N. Alvarado, Á. Leiva, D. Radić, C. Alvarez-Lorenzo, and A. Concheiro, *Encapsulation of antioxidant gallate derivatives in biocompatible poly(ε-caprolactone)-b-pluronic-b-poly(ε-caprolactone) micelles.* Langmuir, 2016. **32**(14): p. 3331-3339.
34. Lee, J.I. and H.S. Yoo, *Biodegradable microspheres containing poly(ε-caprolactone)–pluronic block copolymers for temperature-responsive release of proteins.* Colloids and Surfaces B: Biointerfaces, 2008. **61**(1): p. 81-87.
35. Molau, G.E., *Colloidal and morphological behavior of block and graft copolymers*, in *Block polymers: Proceedings of the symposium on block polymers at the meeting of the american chemical society in new york city in september 1969*, S.L. Aggarwal, Editor. 1970, Springer US: Boston, MA. p. 79-106.

36. Hecht, E. and H. Hoffmann, *Interaction of aba block copolymers with ionic surfactants in aqueous solution.* Langmuir, 1994. **10**(1): p. 86-91.
37. Balsara, N., M. Tirrell, and T. Lodge, *Micelle formation of bab triblock copolymers in solvents that preferentially dissolve the a block.* Macromolecules, 1991. **24**(8): p. 1975-1986.
38. Breiner, U., U. Krappe, V. Abetz, and R. Stadler, *Cylindrical morphologies in asymmetric abc triblock copolymers.* Macromolecular Chemistry and Physics, 1997. **198**(4): p. 1051-1083.
39. Riess, G., *Micellization of block copolymers.* Progress in Polymer Science, 2003. **28**(7): p. 1107-1170.
40. Adams, D.J. and P.D. Topham, *Assembly of block copolymers*, in *Supramolecular chemistry*. 2012, John Wiley & Sons, Ltd.
41. Bernstein, R., C. Cruz, D. Paul, and J. Barlow, *Lcst behavior in polymer blends.* Macromolecules, 1977. **10**(3): p. 681-686.
42. Zhang, Q., C. Weber, U.S. Schubert, and R. Hoogenboom, *Thermoresponsive polymers with lower critical solution temperature: From fundamental aspects and measuring techniques to recommended turbidimetry conditions.* Materials Horizons, 2017. **4**(2): p. 109-116.
43. Ougizawa, T., T. Inoue, and H.W. Kammer, *Ucst and lcst behavior in polymer blends.* Macromolecules, 1985. **18**(10): p. 2089-2092.
44. Ward, M.A. and T.K. Georgiou, *Thermoresponsive polymers for biomedical applications.* Polymers, 2011. **3**(3): p. 1215.
45. Kjellander, R. and E. Florin, *Water structure and changes in thermal stability of the system poly(ethylene oxide)-water.* Journal of the Chemical Society, Faraday Transactions 1: Physical Chemistry in Condensed Phases, 1981. **77**(9): p. 2053-2077.
46. Southall, N.T., K.A. Dill, and A.D.J. Haymet, *A view of the hydrophobic effect.* The Journal of Physical Chemistry B, 2002. **106**(3): p. 521-533.
47. Seuring, J. and S. Agarwal, *Polymers with upper critical solution temperature in aqueous solution.* Macromolecular Rapid Communications, 2012. **33**(22): p. 1898-1920.
48. Bohorquez, M., C. Koch, T. Trygstad, and N. Pandit, *A study of the temperature-dependent micellization of pluronic f127.* Journal of Colloid and Interface Science, 1999. **216**(1): p. 34-40.
49. Mortensen, K., *Structural studies of aqueous solutions of peo-ppo-peo triblock copolymers, their micellar aggregates and mesophases; a small-angle neutron scattering study.* Journal of Physics: Condensed Matter, 1996. **8**(25A): p. A103.
50. Svensson, B., U. Olsson, and P. Alexandridis, *Self-assembly of block copolymers in selective solvents: Influence of relative block size on phase behavior.* Langmuir, 2000. **16**(17): p. 6839-6846.
51. Owens Iii, D.E. and N.A. Peppas, *Opsonization, biodistribution, and pharmacokinetics of polymeric nanoparticles.* International Journal of Pharmaceutics, 2006. **307**(1): p. 93-102.
52. Lee, J.H., J. Kopecek, and J.D. Andrade, *Protein-resistant surfaces prepared by peo-containing block copolymer surfactants.* Journal of Biomedical Materials Research, 1989. **23**(3): p. 351-368.
53. Schmolka, I.R., *Artificial skin i. Preparation and properties of pluronic f‐127 gels for treatment of burns.* Journal of biomedical materials research, 1972. **6**(6): p. 571-582.
54. Woodruff, M.A. and D.W. Hutmacher, *The return of a forgotten polymer—polycaprolactone in the 21st century.* Progress in Polymer Science, 2010. **35**(10): p. 1217-1256.
55. Koleske, J.V., *Chapter 22 - blends containing poly(ε-caprolactone) and related polymers a2 - paul, d.R*, in *Polymer blends*, S. Newman, Editor. 1978, Academic Press. p. 369-389.
56. Luciani, A., V. Coccoli, S. Orsi, L. Ambrosio, and P.A. Netti, *Pcl microspheres based functional scaffolds by bottom-up approach with predefined microstructural properties and release profiles.* Biomaterials, 2008. **29**(36): p. 4800-4807.
57. Cammas, S., K. Suzuki, C. Sone, Y. Sakurai, K. Kataoka, and T. Okano, *Thermo-responsive polymer nanoparticles with a core-shell micelle structure as site-specific drug carriers.* Journal of Controlled Release, 1997. **48**(2): p. 157-164.
58. Jones, M.-C. and J.-C. Leroux, *Polymeric micelles – a new generation of colloidal drug carriers.* European Journal of Pharmaceutics and Biopharmaceutics, 1999. **48**(2): p. 101-111.

59. La, S.B., T. Okano, and K. Kataoka, *Preparation and characterization of the micelle-forming polymeric drug indomethacin-incorporated poly(ethylene oxide)-poly(beta-benzyl l-aspartate) block copolymer micelles.* J Pharm Sci, 1996. **85**(1): p. 85-90.
60. Alargova, R.G., I.I. Kochijashky, M.L. Sierra, K. Kwetkat, and R. Zana, *Mixed micellization of dimeric (gemini) surfactants and conventional surfactants.* Journal of Colloid and Interface Science, 2001. **235**(1): p. 119-129.
61. Xu, W., P. Ling, and T. Zhang, *Polymeric micelles, a promising drug delivery system to enhance bioavailability of poorly water-soluble drugs.* Journal of Drug Delivery, 2013. **2013**: p. 15.
62. Desai, P.R., N.J. Jain, R.K. Sharma, and P. Bahadur, *Effect of additives on the micellization of peo/ppo/peo block copolymer f127 in aqueous solution.* Colloids and Surfaces A: Physicochemical and Engineering Aspects, 2001. **178**(1–3): p. 57-69.
63. Kim, T.-H., Y.-S. Han, J.-D. Jang, and B.-S. Seong, *Sans study on self-assembled structures of pluronic f127 triblock copolymer induced by additives and temperaturethis article will form part of a virtual special issue of the journal, presenting some highlights of the 15th international small-angle scattering conference (sas2012). This special issue will be available in early 2014.* Journal of Applied Crystallography, 2014. **47**(1): p. 53-59.
64. Mata, J.P., P.R. Majhi, C. Guo, H.Z. Liu, and P. Bahadur, *Concentration, temperature, and salt-induced micellization of a triblock copolymer pluronic l64 in aqueous media.* Journal of Colloid and Interface Science, 2005. **292**(2): p. 548-556.
65. Israelachvili, J.N., D.J. Mitchell, and B.W. Ninham, *Theory of self-assembly of hydrocarbon amphiphiles into micelles and bilayers.* Journal of the Chemical Society, Faraday Transactions 2: Molecular and Chemical Physics, 1976. **72**(0): p. 1525-1568.
66. Giacomelli, F.C., I.C. Riegel, C.L. Petzhold, N.P. da Silveira, and P. Štěpánek, *Aggregation behavior of a new series of aba triblock copolymers bearing short outer a blocks in b-selective solvent: From free chains to bridged micelles.* Langmuir, 2009. **25**(2): p. 731-738.
67. Hoare, T.R. and D.S. Kohane, *Hydrogels in drug delivery: Progress and challenges.* Polymer, 2008. **49**(8): p. 1993-2007.
68. Escobar-Chávez, J.J., M. López-Cervantes, A. Naik, Y. Kalia, D. Quintanar-Guerrero, and A. Ganem-Quintanar, *Applications of thermo-reversible pluronic f-127 gels in pharmaceutical formulations.* Journal of Pharmacy & Pharmaceutical Sciences, 2006. **9**(3): p. 339-358.
69. Rowley, J.A., G. Madlambayan, and D.J. Mooney, *Alginate hydrogels as synthetic extracellular matrix materials.* Biomaterials, 1999. **20**(1): p. 45-53.
70. Burdick, Jason A., Robert L. Mauck, and S. Gerecht, *To serve and protect: Hydrogels to improve stem cell-based therapies.* Cell Stem Cell, 2016. **18**(1): p. 13-15.
71. Purcell, B.P., D. Lobb, M.B. Charati, S.M. Dorsey, R.J. Wade, K.N. Zellars, H. Doviak, S. Pettaway, C.B. Logdon, J.A. Shuman, P.D. Freels, J.H. Gorman Iii, R.C. Gorman, F.G. Spinale, and J.A. Burdick, *Injectable and bioresponsive hydrogels for on-demand matrix metalloproteinase inhibition.* Nat Mater, 2014. **13**(6): p. 653-661.
72. Peng, S., J.-Y. Lin, M.-H. Cheng, C.-W. Wu, and I.M. Chu, *A cell-compatible peo–ppo–peo (pluronic®)-based hydrogel stabilized through secondary structures.* Materials Science and Engineering: C, 2016. **69**: p. 421-428.
73. Jang, W.-D., D.-L. Jiang, and T. Aida, *Dendritic physical gel: Hierarchical self-organization of a peptide-core dendrimer to form a micrometer-scale fibrous assembly.* Journal of the American Chemical Society, 2000. **122**(13): p. 3232-3233.
74. Petka, W.A., J.L. Harden, K.P. McGrath, D. Wirtz, and D.A. Tirrell, *Reversible hydrogels from self-assembling artificial proteins.* Science, 1998. **281**(5375): p. 389-392.
75. Deng, G., C. Tang, F. Li, H. Jiang, and Y. Chen, *Covalent cross-linked polymer gels with reversible sol− gel transition and self-healing properties.* Macromolecules, 2010. **43**(3): p. 1191-1194.
76. Lin, H.-H. and Y.-L. Cheng, *In-situ thermoreversible gelation of block and star copolymers of poly (ethylene glycol) and poly (n-isopropylacrylamide) of varying architectures.* Macromolecules, 2001. **34**(11): p. 3710-3715.

77. Liu, C.B., C.Y. Gong, M.J. Huang, J.W. Wang, Y.F. Pan, Y.D. Zhang, G.Z. Li, M.L. Gou, K. Wang, M.J. Tu, Y.Q. Wei, and Z.Y. Qian, *Thermoreversible gel-sol behavior of biodegradable pcl-peg-pcl triblock copolymer in aqueous solutions.* J Biomed Mater Res B Appl Biomater, 2008. **84**.
78. Khorshid, N.K., K. Zhu, K.D. Knudsen, S. Bekhradnia, S.A. Sande, and B. Nyström, *Novel structural changes during temperature-induced self-assembling and gelation of plga-peg-plga triblock copolymer in aqueous solutions.* Macromolecular Bioscience, 2016. **16**(12): p. 1838-1852.
79. Jeong, B., Y.H. Bae, and S.W. Kim, *Thermoreversible gelation of peg−plga−peg triblock copolymer aqueous solutions.* Macromolecules, 1999. **32**(21): p. 7064-7069.
80. Nyström, B., A.-L. Kjøniksen, and B. Lindman, *Effects of temperature, surfactant, and salt on the rheological behavior in semidilute aqueous systems of a nonionic cellulose ether.* Langmuir, 1996. **12**(13): p. 3233-3240.
81. Pandit, N.K. and J. Kisaka, *Loss of gelation ability of pluronic® f127 in the presence of some salts.* International Journal of Pharmaceutics, 1996. **145**(1): p. 129-136.
82. Cabana, A., A. Aït-Kadi, and J. Juhász, *Study of the gelation process of polyethylene oxidea–polypropylene oxideb–polyethylene oxideacopolymer (poloxamer 407) aqueous solutions.* Journal of Colloid and Interface Science, 1997. **190**(2): p. 307-312.
83. López-Barrón, C.R., N.J. Wagner, and L. Porcar, *Layering, melting, and recrystallization of a close-packed micellar crystal under steady and large-amplitude oscillatory shear flows.* Journal of Rheology, 2015. **59**(3): p. 793-820.
84. Kjøniksen, A.-L., K. Zhu, R. Pamies, and B. Nyström, *Temperature-induced formation and contraction of micelle-like aggregates in aqueous solutions of thermoresponsive short-chain copolymers.* The Journal of Physical Chemistry B, 2008. **112**(11): p. 3294-3299.
85. Grillo, I., *Small-angle neutron scattering and applications in soft condensed matter*, in *Soft matter characterization*, R. Borsali and R. Pecora, Editors. 2008, Springer Netherlands: Dordrecht. p. 723-782.
86. Chu, B., *Dynamic light scattering*, in *Soft matter characterization*, R. Borsali and R. Pecora, Editors. 2008, Springer Netherlands: Dordrecht. p. 335-372.
87. Hammouda, B. *Probing nanoscale structures - the sans toolbox*. 2008.
88. Pecora, R., *Dynamic light scattering: Applications of photon correlation spectroscopy*. 1985: Springer.
89. Miller, C.C., *The stokes-einstein law for diffusion in solution.* Proceedings of the Royal Society of London. Series A, 1924. **106**(740): p. 724-749.
90. Siegert, A.J.F., *On the fluctuations in signals returned by many independently moving scatterers*. 1943, [Cambridge, Mass.: Radiation Laboratory, Massachusetts Institute of Technology.
91. Kjøniksen, A.-L., B. Nyström, and B. Lindman, *Effects of temperature, surfactant concentration, and salinity on the dynamics of dilute solutions of a nonionic cellulose derivative.* Langmuir, 1998. **14**(18): p. 5039-5045.
92. Lauten, R.A., A.-L. Kjøniksen, and B. Nyström, *Adsorption and desorption of unmodified and hydrophobically modified ethyl(hydroxyethyl)cellulose on polystyrene latex particles in the presence of ionic surfactants using dynamic light scattering.* Langmuir, 2000. **16**(10): p. 4478-4484.
93. Brown, W., K. Schillen, M. Almgren, S. Hvidt, and P. Bahadur, *Micelle and gel formation in a poly (ethylene oxide)/poly (propylene oxide)/poly (ethylene oxide) triblock copolymer in water solution: Dynamic and static light scattering and oscillatory shear measurements.* The Journal of Physical Chemistry, 1991. **95**(4): p. 1850-1858.
94. Claro, B.M.A.G.M., *Phase behavior, microstructure and cytotoxicity in mixtures of a charged triblock copolymer and surfactant*, in *Departamento de Quimica e Bioquimica*. 2015, Universidade de Porto: Porto. p. 115.
95. Higgins, J.S., *Polymers and neutron scattering*.
96. Barnes, H.A., *A handbook of elementary rheology*. 2000: University of Wales, Institute of Non-Newtonian Fluid Mechanics.

97. Mezger, T.G., *The rheology handbook, 4th edition*. 2014: Vincentz Network, United States.
98. Ferry, J.D., *Viscoelastic properties of polymers*. 1980: John Wiley & Sons.
99. Larson, R.G., *The structure and rheology of complex fluids*. 1999, New York: Oxford University Press.
100. WEITZ, D., H. WYSS, and R. LARSEN, *Oscillatory rheology: Measuring the viscoelastic behaviour of soft materials.* GIT laboratory journal Europe, 2007. **11**(3-4): p. 68-70.
101. Winter, H.H. and F. Chambon, *Analysis of linear viscoelasticity of a crosslinking polymer at the gel point.* Journal of rheology, 1986. **30**(2): p. 367-382.
102. Zhou, J., G. Wang, L. Zou, L. Tang, M. Marquez, and Z. Hu, *Viscoelastic behavior and in vivo release of microgel dispersions with inverse thermo-reversible gelation.* Biomacromolecules, 2008. **9**(1): p. 142-148.
103. Tanodekaew, S., J. Godward, F. Heatley, and C. Booth, *Gelation of aqueous solutions of diblock copolymers of ethylene oxide and d,l‐lactide.* Macromolecular Chemistry and Physics, 1997. **198**(11): p. 3385-3395.
104. Dormidontova, E.E., *Role of competitive peo−water and water−water hydrogen bonding in aqueous solution peo behavior.* Macromolecules, 2002. **35**(3): p. 987-1001.
105. Basak, R. and R. Bandyopadhyay, *Encapsulation of hydrophobic drugs in pluronic f127 micelles: Effects of drug hydrophobicity, solution temperature, and ph.* Langmuir, 2013. **29**(13): p. 4350-4356.
106. Bayati, S., K. Zhu, L.T.T. Trinh, A.-L. Kjøniksen, and B. Nyström, *Effects of temperature and salt addition on the association behavior of charged amphiphilic diblock copolymers in aqueous solution.* The Journal of Physical Chemistry B, 2012. **116**(36): p. 11386-11395.
107. Attwood, D., J. Collett, and C. Tait, *The micellar properties of the poly (oxyethylene)-poly (oxypropylene) copolymer pluronic f127 in water and electrolyte solution.* International journal of pharmaceutics, 1985. **26**(1-2): p. 25-33.
108. Nyström, B. and H. Walderhaug, *Dynamic viscoelasticity of an aqueous system of a poly(ethylene oxide)−poly(propylene oxide)−poly(ethylene oxide) triblock copolymer during gelation.* The Journal of Physical Chemistry, 1996. **100**(13): p. 5433-5439.
109. Castelletto, V., I.W. Hamley, X.F. Yuan, A. Kelarakis, and C. Booth, *Structure and rheology of aqueous micellar solutions and gels formed from an associative poly(oxybutylene)-poly(oxyethylene)-poly(oxybutylene) triblock copolymer.* Soft Matter, 2005. **1**(2): p. 138-145.
110. Pedersen, J.S. and M.C. Gerstenberg, *Scattering form factor of block copolymer micelles.* Macromolecules, 1996. **29**(4): p. 1363-1365.
111. Livsey, I., *Neutron scattering from concentric cylinders. Intraparticle interference function and radius of gyration.* Journal of the Chemical Society, Faraday Transactions 2: Molecular and Chemical Physics, 1987. **83**(8): p. 1445-1452.
112. Roe, R.-J., *Methods of x-ray and neutron scattering in polymer science*. Vol. 739. 2000: Oxford University Press on Demand.

Appendix A: Theoretical Model for Spherical Core-Shell Micelles

According to Pedersen & Gerstenberg [110], the form factor of a micelle can be written as a sum of four different terms: the self- correlation term of the core, the self-correlation term of the chains, the cross-term between the core and chains, and the cross term between different chains.

$$F_{mic}(q) = N^2\beta_s^2 F_s(q) + N\beta_c^2 F_c(q) + 2N^2\beta_s\beta_c S_{sc}(q) + N(N-1)\beta_c^2 S_{cc}(q) \quad (21)$$

For diblock copolymers N is the aggregation number of the micelle and β_s and β_c are the total excess scattering lengths of a block in the core and in the corona, respectively. They can be calculated as $\beta_s = V_s (\rho_s - \rho_{solv})$ and $\beta_c = V_c (\rho_c - \rho_{solv})$, respectively, where Vs and Vc are the total volumes of a block in the core and in the corona. ρ_s and ρ_c are the corresponding scattering length densities and ρ_{solv} is the scattering length density of the solvent. Here F_s(q)

$$F_s(q) = \Phi^2(qR) \quad (22)$$

where ϕ (qR) is the form factor of a sphere given by

$$\Phi(qR) = \frac{3[\sin(qR) - qR\cos(qR)]}{(qR)^3} \quad (23)$$

The chains in the corona have a radius of gyration Rg and the self-correlation term of the Gaussian chains is, with $x = (qR_g)^2$, given by

$$F_c(q) = \frac{2[\exp(-x) - 1 + x]}{x^2} \quad (24)$$

Furthermore, the interference cross term between the core and the chains is given by

$$S_{sc}(q) = \Phi(qR)\psi(qR_g)\frac{\sin(q[R+dR_g])}{q[R+dR_g]} \qquad (25)$$

where the parameter *d* has been introduced to mimic non-penetration of the Gaussian chains into the core. They are therefore taken as starting a distance *d* times R_g away from the surface of the core, where *d* is close to unity. The function $\Psi(x)=[1-\exp(-x)]/x$ is the form factor amplitude of the chain.

Appendix B: Core-shell cylinder model

The form factor is in this case calculated as [111]:

$$P(q) = \frac{scale}{V_{shell}} \int_0^{\pi/2} f^2(q,\alpha) \sin\alpha \, d\alpha \tag{26}$$

$$f(q,\alpha) = 2(\rho_{core} - \rho_{shell}) V_{core} j_0(qH\cos\alpha) \frac{J_1(qr\sin\alpha)}{(qr\sin\alpha)} + 2(\rho_{shell} - \rho_{solvent}) V_{shell} j_0[q(H+t)\cos\alpha] \frac{J_1[q(r+t)\sin\alpha]}{[q(r+t)\sin\alpha]} \tag{27}$$

$$j_0(x) = \sin(x)/x, \quad V_{core} = \pi r^2 L \quad \text{and} \quad V_{shell} = \pi(r+t)^2 L_{total}$$

where r is the radius of the core of the cylinder, *t* the thickness of the shell. L is the length of the cylinder and *H* is the half-length. $J_1(x)$ is the first order Bessel function. α is the angle between the cylinder axis and the scattering vector, *q*. V_{shell} is the volume of the cylinder shell and V_{core} that of the core. The integral over alpha averages the form factor over all possible orientations of the cylinder.

Appendix C: Polymer chain model

The form factor is in this case given by the Debye function representing a linear chain [112]:

$$D(x) = 2(e^{-x} + x - 1)/x^2 \tag{28}$$

where with x = $(qR_g)^2$.

In this case R_g is the only parameter fitted considering that q is given.